PHASE SELECTION MECHANISMS IN ISOCHRONOUS CYCLOTRONS PRODUCING HIGH RESOLUTION BEAMS

By

John Curtis Collins

A THESIS

Submitted to
Michigan State University
in partial fulfillment of the requirements
for the degree of

DOCTOR OF PHILOSOPHY

Department of Physics

1973

ABSTRACT

PHASE SELECTION MECHANISMS
IN ISOCHRONOUS CYCLOTRONS
PRODUCTING HIGH RESOLUTION BEAMS

By

John Curtis Collins

Phase selection utilizing coupling between radial and longitudinal motion has long been a useful tool at the Michigan State University Isochronous Cyclotron for producing very high energy-resolution beams. A study was undertaken to obtain a better understanding of this phenomenon by identifying the relevant machine parameters and their quantitative effects. While the M.S.U. machine provides a convenient prototype cyclotron, our results are not confined to this one example as various dee angles and magnetic field structures are investigated. Other parameters of importance are dee voltage, acceleration harmonic and phase history. The role of orbit centering is given particular attention, especially as it relates to the difference between actual phase histories and those from the standard M.S.U. field trimming program. Most orbit calculations were done with a precise numerical integration code limited only by the assumption of step function energy gain. Finally, the data is used to discuss the general problem of placement and effectiveness of phase selection slits.

ACKNOWLEDGEMENTS

I would like to take this opportunity to thank Julie Perkins for invaluable help and advice in the preparation of this manuscript.

I would also like to thank Richard Au and Dave Johnson for their time and aid in computer programming and the use of orbit codes.

Thanks are due also to Larry Learn and Dr. Henry Blosser for many helpful discussions and explanations of cyclotron theory and operations.

My special thanks go to Dr. Morton Gordon whose patient guidance gave this work direction and purpose and to my wife Carolyn, whose impatient prodding kept the work moving along. This thesis could not have been finished without both of these people.

Finally, I wish to acknowledge the financial support of the National Science Foundation throughout my graduate career.

TABLE OF CONTENTS

LIST OF FIGURES

LIST OF TABLES

1. INTRODUCTION

1.1 Historical Background

Most cyclotrons operating normally are high current, imprecise beam sources exhibiting large emittances (40 mm-mr is not atypical) and beam pulse phase widths (typically 20^{o} to 30^{o} phase widths corresponding to microscopic duty factors of 6 to 8%). Such beams prove difficult to extract cleanly and multi-turn extraction is commonplace (with efficiencies of 50-70%), but with the consequence that the external beam has an energy spread of approximately the internal energy gain per turn. On the other hand, modern nuclear physics experiments require small beam spots and energy widths to obtain their ultimate resolution. This conflict is usually resolved by designing the external beam handling system with analyzing magnets and slits to strip away unwanted particles. This technique involves large aperture (expensive) magnets or high background radiation and residual activity or, regretably, both.

A different solution is to obtain small emittance and good energy resolution by extracting only a single turn (at nearly 100% efficiency). The external beam would then be an "image" of the ion source, which could be constructed with a small slit to give small emittance. An energy spread would still arise because of the sinusoidal

variation of the accelerating voltage with time but, while possibly larger than desired, this would be much smaller than the energy gain per turn. The fractional energy spread generated in this way for a beam phase width of $2\Delta\phi$ in a perfectly isochronous field is:[1]

$$\Delta E/E = (\Delta\phi)^2/2. \qquad (1)$$

From extensive studies,[2] it was confirmed that single turn extraction requires small $\Delta\phi$. Not independently one notices from Eq. (1) that this also produces superior energy resolution. The question then is how to obtain such small phase widths.

Three methods have been used to accomplish this selection of desired phase at M.S.U. The original idea was to use the phase dependent axial focusing properties of the electric field at the first few gaps with an axial slit.[3] This system produced phase widths of about 7^{o}, good enough to observe single turn extraction. However, Eq. (1) indicates that it is profitable to attempt to reduce this phase width as much as possible. It was also true that the axial slit passed particles of any phase if they were emitted with small axial momentum near the median plane. Analysis of certain empirical data showed that radial slits at the half and tenth turns gave better phase selection.[4] Such a system worked through the coupling between the radial and longitudinal (E-ϕ) motions of the

particles and produced approximately 3.5° phase widths, a substantial improvement.

The third method, and the one presently in use, is a refinement of the second retaining the half turn slit and locating two more radial slits on turns 18 and 28.[5] Beam pulse widths are now observed as low as 1.4° FWHM with radial emittances of less than 1.0 mm-mr. These slits thus make the M.S.U. machine a very precise nuclear physics instrument. The position of these slits on early turns also means that very little bothersome background radiation is produced.

The precise mechanism of the longitudinal-radial coupling responsible for phase selection has not been fully delineated to this point. It was therefore decided that a general study would be useful to determine which cyclotron parameters affect this coupling, what the mechanism of the effect is and how successful a system of phase selective slits would be in other cyclotrons of various design. This paper presents the results of that investigation.

1.2 The Approach to the Problem

The data presented herein is intended as only a very rough guide to the importance of the parameters investigated and the effectiveness of phase selection slits under specified conditions. We have neglected details of source and early turn electric fields which would have important consequences in real cyclotrons but which would also be different in every machine. What we wish to emphasize are the methods we use to analyze the longitudinal-radial coupling since these apply universally and serve as a very handy visualization of the coupling process.

The inclusion of phase selection slits allows us to define a central ray from ion source to extractor. This is done in Sec. 2.1. This central ray plays a crucial role in this analysis, as it does in the design and operation of any cyclotron built for high resolution. From one point of view, a real beam is built up around the central ray through small variations in position, momentum and phase, so that beam properties in general and the properties of individual particles in the beam should be intimately related to the characteristics of the central ray.

We investigated various dee angles between 180° and 90° since most existing cyclotrons use 180° dees with some (Maryland being the prime example) using 90° dees and a few using 150° or 120° dees. Both three and four sector magnetic fields are used and acceleration harmonics one, two and three were looked at. Other parameters

judged to be of general interest or possible heuristic importance were energy gain per turn, average phase history near machine center and relative orientation between the dees and the field sector structure.

Our data on the longitudinal-radial coupling are expressed in terms of the radial separation between the central ray and a ray differing from it in initial phase. In Chapter 2 we resolve this radius difference into two components: the first depending on the total energy difference between the rays and the second depending on the details of how this energy difference was achieved. We then discuss various properties of these components, including their dependence on turn number, and detail the role of the central ray. In Chapter 3 we analyze our computer generated data in the framework provided by Chapter 2 to determine how each component depends on the various cyclotron parameters.

2. ORBIT PROPERTIES AND CALCULATIONS

2.1 Introductory Mechanics

To facilitate the study of particle orbits and their differences, we may resolve the radial position of a particle of energy E at azimuth θ, $r(E,\theta)$, into two components. The first is the static equilibrium orbit (EO) radius, $R_{EO}(E,\theta)$; the second is the deviation from that EO value

$$x = r(E,\theta) - R_{EO}(E,\theta).$$

For any energy E we may define the EO in a magnetic field as the non-accelerated closed orbit having the same periodicity as the field. This analysis proves useful because the EO is a function only of azimuth and total energy (see Sec. 2.5). Thus we may separate out purely energy effects in the radial differences between particles. The canonically conjugate variable, p_r, the radial component of momentum, is likewise resolved such that

$$p_x = p_r(E,\theta) - P_{REO}(E,\theta).$$

Of course, x and p_x are also functions of energy and azimuth, but we choose not to include that dependence in our notation. Since x and p_x have equal footing in this formulation, it is highly convenient to express them in the same units.

We choose to use mils (1 mil=0.001 in.=0.0254 mm) and transform p_x from classical units into these units using $p_x(\text{mils}) = (A/m_o c)\ p_x$, where m_o is the rest mass of the particle under consideration and A is the cyclotron length unit (= c/ω_o where ω_o is the ideal isochronous orbital frequency) expressed in mils.

Completing the dynamical description of a particle requires the conjugate variable pairs (t,E) and (z,p_z). These, with (r,p_r) or equivalently, (x,p_x), define a six dimensional phase space for the particle. We choose to express the time t in terms of the phase angle ϕ defined here as

$$\phi = \theta_{rf} - h\theta = \omega_{rf}t - h\theta,$$

where ω_{rf} is the frequency of the accelerating voltage and h is the acceleration harmonic, i.e., $h = \omega_{rf}/\omega_o$.

We neglect z motion entirely. This is justified as long as we are considering motion near the median plane. This condition implies that the maximum phase change per turn expected from axial motion for a maximum vertical amplitude d, given by

$$\delta_z\phi \leq 2\pi h\ (\nu_z d/2R_{EO})^2,$$

will always be small.

The static EO we have defined is a very useful tool in analyzing single particle motion in sectored magnetic

fields, partly because one may visualize x and p_x values as specifying the deviation of the actual particle orbit center from the magnetic field center, and partly because one can show that a particle coasting in the vicinity of a reference EO of the same energy executes harmonic (betatron) oscillations about that EO.[6] In the x-p_x plane centered on this EO, the phase point for the coasting particle rotates about the origin at a distance equal to the precessional oscillation amplitude and at a rate such that, at a given azimuth the phase point returns to its original position after $1/(\nu_r-1)$ orbits (turns) in the field. If one observes the location of such a phase point over many turns at a fixed azimuth relative to each field sector, one finds that an eigen-ellipse is traced out. The ellipse is a function of azimuth arising from the periodicity of the magnetic field through Floquet's theorem. Detailed accounts of its properties may be found elsewhere,[7,8,9] and will not be reproduced here. As an example, one such ellipse is traced out in Fig. 1a for a proton of 14 MeV coasting in a field corresponding to a maximum energy of 30 MeV. (See Sec. 2.2 for the source of this field.) Initial conditions used are x=20 mils and p_x=0 mils and $\nu_r \simeq 1.05$.

Since particles execute betatron oscillations about any orbit which satisfies the equations of motion in the given field, we are not limited to the static EO as our

Figure 1.--X(mils) vs. P_x(mils) for a 14 MeV proton in a three sector, 30 MeV field. Points are plotted once per turn at $\theta=0^o$ for no acceleration (a) and acceleration of 143 keV/turn with two 138^o dees located symmetrically relative to $\theta=0^o$ (b).

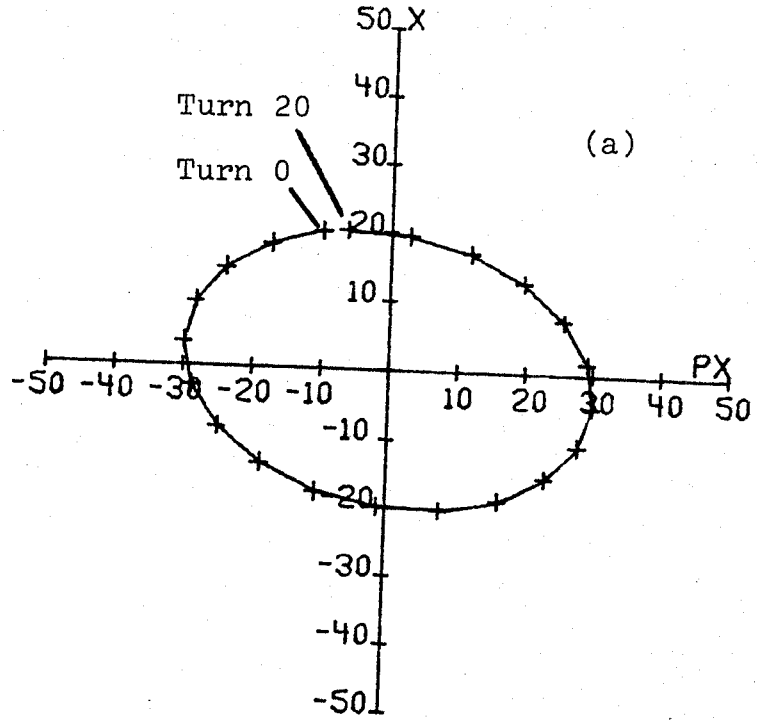
50 X
40
30
20
10
-10
-20
-30
-40
-50
Turn 20
Turn 0
(a)
PX
-50 -40 -30 -20 -10
10 20 30 40 50

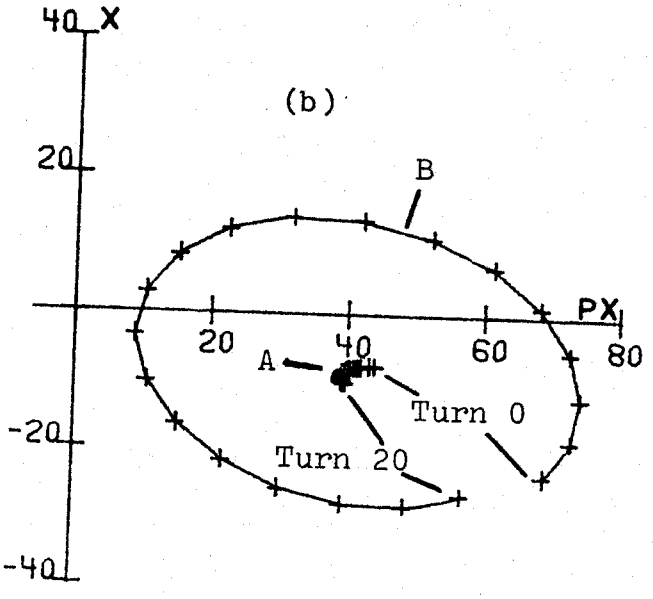
40 X
(b)
20
-20
-40
B
A
PX
20 40 60 80
Turn 0
Turn 20

Figure 1.

choice of phase space origin, while still maintaining the characteristics of the phase point motion described above. That other choices might be advantageous should be obvious since we have not yet mentioned the acceleration process. In a separated turn machine, it is highly useful to define an accelerated equilibrium orbit (AEO).[1] Just as the static EO is closed in configuration space, the AEO is taken to be that path of an accelerated particle which is closed after one turn in the x-p_x plane, i.e., the representative phase point is a "fixed point".

To illustrate the value of the AEO, Fig. 1b shows the motions for two phase points representing protons accelerated in the same field as used in Fig. 1a: particle A started (x=-7.6 mils, p_x=42.5 mils, E=13 MeV) such that it passes along an AEO on its seventh turn (=14 MeV) and particle B started (x=-23.5 mils, p_x=68.3, E=13 MeV) such that after seven turns it is displaced by δx=20 mils and δp_x=0 mils from the AEO of 14 MeV. Comparing the path followed by B with that in Fig. 1a, we see that the AEO acts as a center of oscillation for accelerated particles displaced from it just as the EO (origin in Fig. 1a) did before.

Were we to consider two beams filling identical ellipses in the x-p_x plane, one centered on A, the other on B, that centered on B would effectively fill a phase space area larger than the beam ellipse itself and exhibit coherent

radial oscillations as B traverses the path shown for it. The beam ellipse centered on A would effectively occupy an area only slightly larger than itself since A does not move far in the $x\text{-}p_x$ plane. This is true regardless of incoherent variations inside each ellipse. The beam corresponding to the ellipse centered on A may be termed "well-centered". In fact, at a given energy and phase, the beam centered on the appropriate AEO will show the minimum possible coherent oscillation amplitude. While this condition holds exactly at only one energy, the coherent oscillation amplitude increases only slowly with deviations from the energy of the selected AEO, so that a beam which is well-centered near the middle of its acceleration history will be so throughout its entire history except on the first few turns after the source-puller. Such centering is of great practical importance because it reduces phase oscillations (see Sec. 2.4), minimizes the effects of non-linearities and makes extraction insensitive to dee voltage.

Like the EO, the AEO depends on the magnetic field. But since the AEO characterizes the acceleration process, it is also a function of the dee structure and the particle phase, of which properties the EO is independent. Details of AEO properties of specific importance to this study are given in Sec. 2.3.

Using the AEO of energy E and the corresponding desired phase, we define the "central" ray (CR) as that one which travels along the AEO on some turn near half the final energy. The CR should then be a best centered ray in the sense that any ray with other initial r,p_r values will exhibit larger coherent precessional oscillation amplitude. The precise energy used for the AEO should not be at all critical. The CR might also be termed the "design" ray since it would be used to locate the ion source and any beam slits in a real machine.

2.2 Computation Technique

The information provided above may now be used to guide our design of the calculations required to understand the longitudinal-radial coupling. We are certainly interested in EO and AEO properties as well as in finding a well centered beam. We are also interested in determining how machine design affects these properties and, through them, phase selection. The discussion below of the codes and calculation methods finally used serves to list and fix some limitations on the machine parameters at our disposal, as well as showing how the concepts of the AEO and well centered beam are actually put to use.

Most of the magnetic fields used were obtained using the field trimming program "Fielder".[10] Two Fielder features are particularly convenient for studying the various effects of phase histories: (a) one may specify a desired phase-as-a-function-of-energy curve to which the final field should conform; and (b) an acceleration history of phase and energy vs. turn number (τ) is output along with the field. The phase history, denoted $\phi_F(\tau)$ or $\phi_F(E)$, is quite valuable for estimating one contribution to the longitudinal-radial coupling as shown in Sec. 2.5. It is obtained by assuming that the particle gains energy continuously and always remains on an EO. This is a good approximation for a well centered particle when its energy is very much greater than the maximum energy gain per turn.

But on early turns we shall note large and important differences between actual phases at gap crossings and $\phi_F(\tau)$.

Fielder utilizes measured field data from the M.S.U. cyclotron, so, strictly speaking, our results are limited to isochronous fields of low spiral with central cone and three sectors. However, spiral is very nearly zero near the center of any cyclotron, where phase selective slits would be placed. The cone provides vertical focusing in the central region. Its effect on $\phi_F(\tau)$ may be modified by proper trim coil currents. Lastly, most low energy cyclotrons have three sectors and Fielder does produce an artificial four sector field, so we are not restricted in choice of field periodicity.

As previously mentioned, the AEO at any energy depends on the dee structure involved. Our investigations covered the most widely used dee angles (180^o, 138^o, 90^o). Since, under assumptions given below, the only difference between having one or two 180^o dees lies in the achievable energy gains per turn, we make no distinction between the two cases. Situations with three dees were not considered. Our standard dee set assumes straight edged dee gaps and is described by two angles: the dee angle α subtended by the dee edges and the orientation angle θ_{or} measured from the radius at $\theta=0^o$ in the magnetic field to the line of reflection symmetry between the dees. Since we are using

M.S.U. field data, $\theta=0^{o}$ is positioned near the center of a valley. For convenience we number the accelerating gaps counterclockwise beginning with gap 1 at

$$\theta_1 = \theta_{or} + (\pi-\alpha)/2$$

$$\theta_2 = \theta_{or} + (\pi+\alpha)/2$$

$$\theta_3 = \theta_1 + \pi$$

$$\theta_4 = \theta_2 + \pi.$$

The codes used to calculate particle orbits all use the same exact median plane equations of motion and assume step function energy gain. This assumption is a limitation in applying our quantitative results directly to any real machine if the first few acceleration gaps are included. There, transit time effects are important as they modify the CR x-p_x and phase (energy gain) histories. These effects are so highly dependent on central region geometry, it was thought best to omit them entirely from this work.

The particles are assumed to start from a virtual source at $\theta=\theta_1$ on the first turn ($\tau=0$). We consider 0.9 times the maximum energy gain per gap, E_g, to be a reasonable source-puller or axial injection energy and use this value in step iii) below.

The outline of our calculational procedure is as follows:

i) We obtained a magnetic field from Fielder. The input to Fielder consisted of the field periodicity N,

the particle type (E_o and q), the final energy desired E_f, the approximate number of turns τ_F, the acceleration harmonic h and a phase curve for Fielder to attempt to match. Aside from the desired magnetic field, Fielder supplies EO data (R_{EO}, P_{REO}, ν_r vs. E) for the field, a proper energy gain per turn E_1, ω_{rf} and the actual phase curve $\phi_F(\tau)$.

ii) Using the code "Disport-2",[11] AEO's covering a range of energies including $E_f/2$ were calculated for specified $\phi_F(E)$, α and θ_{or} values. The AEO's are specified by listing their r, p_r, x, p_x, ϕ and E values at each gap, as well as at $\theta=\theta_{or}$ and $\theta=\theta_{or}+\pi$.

iii) Selecting an energy near $E_f/2$ occuring at $\theta=\theta_{or}$, the corresponding r, p_r and ϕ values were used to initiate "acceleration" of a ray backwards by the code "Goblin-4".[11] An adjustment was made to the starting energy so that the corrected Goblin results for the initial energy ($\tau=0$, $\theta=\theta_1$), our last free parameter, would be $0.9\ E_g$. We then interpolated in the AEO table of step ii) to find new starting r and p_r for the adjusted energy and the backward run was repeated. Three or four iterations were usually sufficient to obtain CR starting conditions at $\theta=\theta_1$ in this way.

iv) With the initial CR coordinates (r_i, p_{ri}, ϕ_i, E_i) now determined, we used the code "Devil", written by the author (see Sec. 5.2), to accelerate the CR and rays differing from it slightly by δr_i, δp_{ri} and/or $\delta \phi_i$. Devil output the orbit properties (r, p_r, ϕ, E, x, p_x) at each dee gap and any other azimuths desired (usually θ_{or} and $\theta_{or}+\pi$) along with the differences in r, R_{EO}, x and p_x between the CR and the displaced rays. This output forms the great majority of the data displayed in this thesis.

2.3 The Accelerated Equilibrium Orbit

To provide a framework in which to present our data, it is convenient to discuss some of the properties of the orbits which we shall calculate as outlined in the previous section. In particular, the AEO, the CR and certain properties of the beam surrounding the CR deserve special attention, and in that order, because each item depends intimately on the one preceding it. For the AEO, we are interested in its variations with energy, phase, E_1 and starting azimuth in three and four sector fields.

We can derive a simple formula for the initial conditions of the AEO by using a transfer matrix formalism in which betatron oscillations may be represented as rotation of the vector

$$X = x - i\eta p_x,$$

for $\eta = R_o/(\nu_r p) \simeq 1$ in our units. At each gap, the phase point representing an accelerated particle experiences a shift in the negative x direction equal in magnitude to the corresponding δR_{EO}. If this shift is represented simply as δ, we may determine the initial amplitude X_o for an AEO to be

$$X_o = x_o - i\eta p_{xo} = -i\delta\cos(\nu_r\alpha/2)/\sin(\nu_r\pi/2), \quad (2)$$

(see Sec. 5.1.1). Including the p_x shift which also occurs at each gap would add a small real term to X_o, but little

to our understanding of the AEO, so we shall not treat it specifically. The transfer matrix used here neglects all field structure and is symmetric between half turns, that is, after one half turn, $x=x_o$ and $p_x=p_{xo}$.

Figures 2 and 3 show Disport-2 results for AEO's in 30 MeV proton fields with N=4 and N=3, respectively. The AEO properties are plotted vs. energy at $\alpha=138^o$ and vs. dee angle at E=7.5 MeV, both at $\theta=\theta_{or}=0^o$. We plot the average in mils of the p_x values at $\theta=0^o$ and 180^o for comparison with Eq. (2). The average x values are not included as they never exceed 1.5 mils. To measure orbit asymmetry, i.e., the deviation from Eq. (2), we plot the deviations from the average in x and p_x values at $\theta=0^o$. The x deviations have sign opposite that of the other quantities plotted.

The results in the four sector field are in excellent agreement with Eq. (2) using δ varying as $(\Delta E)\ E^{-\frac{1}{2}}$, where ΔE is taken as the energy gain per turn divided by the number of acceleration gaps (see Sec. 2.5). The asymmetries are quite small, except at rather low energies where the assumption of constant δ begins to fail markedly. Such agreement with Eq. (2) is not too surprising since the field and dee geometries are both symmetric between half turns.

AEO's in a three sector field (Fig. 3) are quite asymmetric, however. Numerical agreement with Eq. (2) is quite poor for both dee angle and energy dependence. Obviously, Eq. (2) makes no allowance for the fact that the

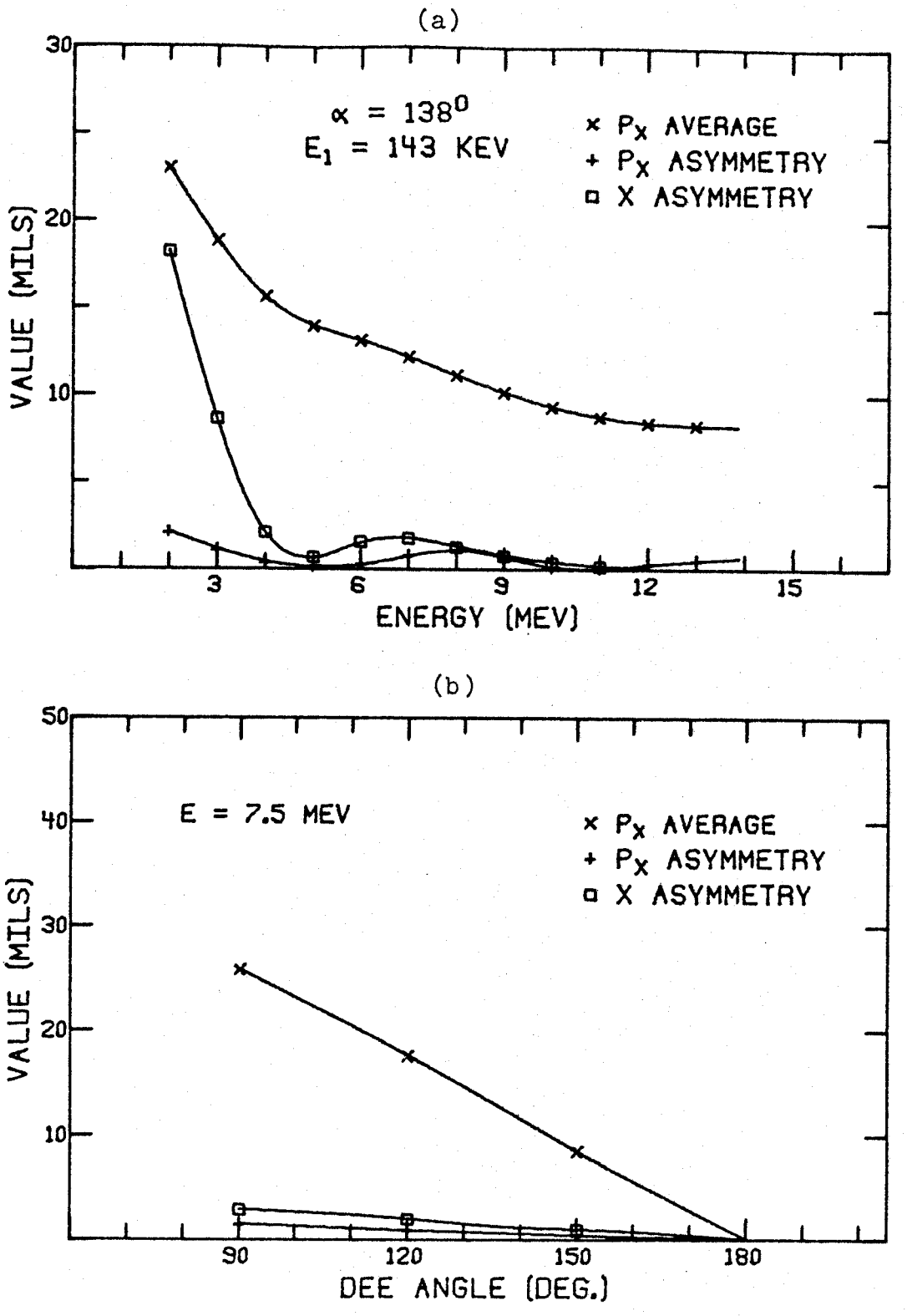

Figure 2. AEO properties in a four sector magnetic field at $\theta=\theta_{or}=0^{\circ}$. "Average" values are the mean of $p_x(0^{\circ})$ and $p_x(180^{\circ})$. Asymmetries are values at 0° minus the average value.

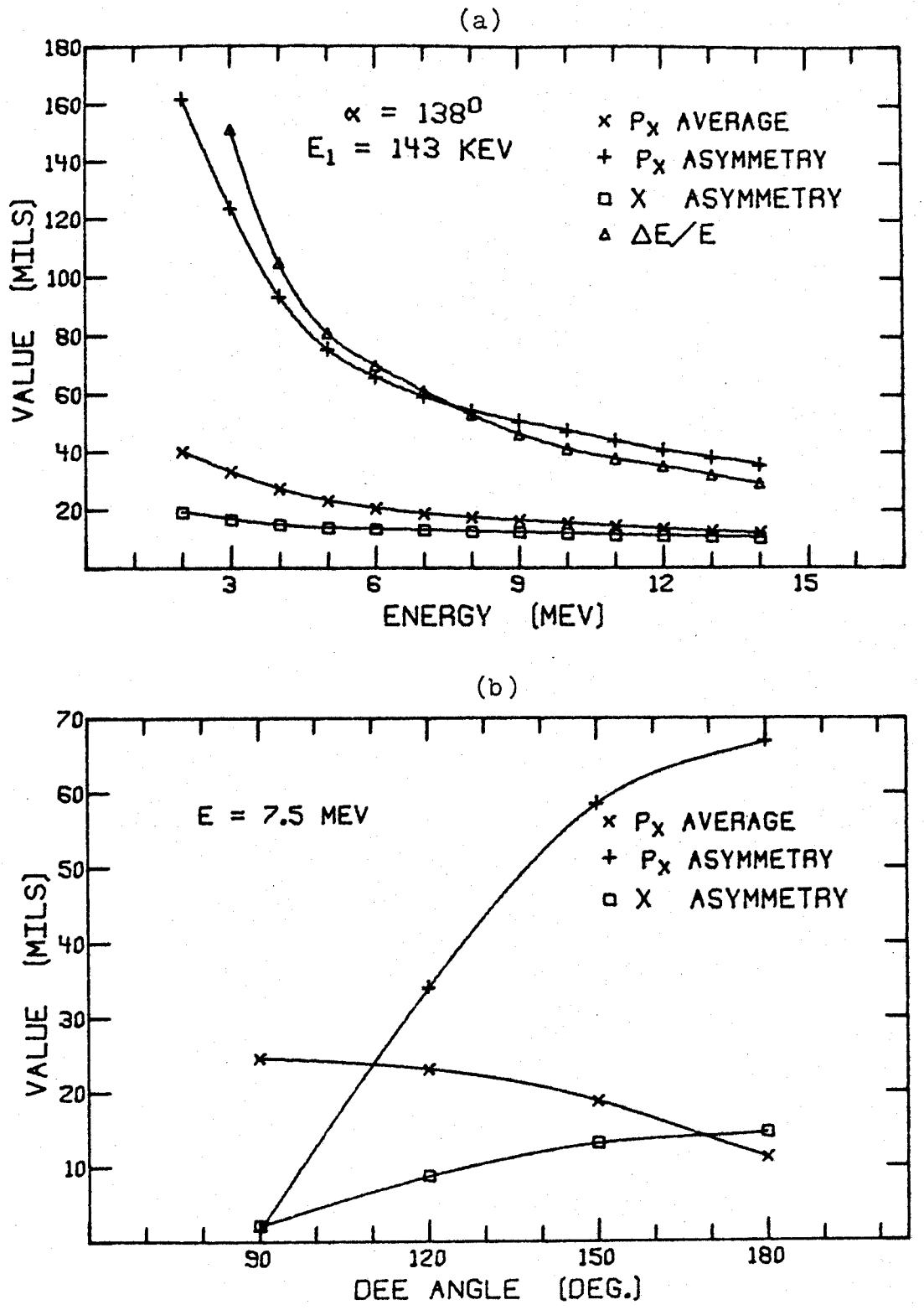

Figure 3. AEO properties as in Fig. 2 except with a three sector magnetic field. Compare the ordinate scales with those in Fig. 2.

transfer matrix is no longer symmetric between half turns because the magnetic field no longer possesses two-fold symmetry. Both asymmetry and average values do vary directly as ΔE and roughly as $\Delta E/E$. The curve labeled "$\Delta E/E$" in Fig. 3a was positioned by choosing a proportionality constant C (=2864 mils) such that, at 7 MeV, the p_x asymmetry value is $C(\Delta E/E)$. (Such behavior is typical of the "gap-crossing" resonance.)[12] Both x and p_x asymmetry values vary as cos α.

Since the four sector field is symmetric about any diameter, changing θ_{or} has no effect on the curves in Fig. 2. However, the three sector field results are functions of θ_{or}, the most striking of which is the reversal of the x and p_x asymmetry values with a 30^o change from $\theta_{or}=0^o$. For both cases, sweeping θ_{or} through one sector causes the phase point representing an AEO to "rotate" about the origin counterclockwise by 360^o. For the four sector field, the point maintains a constant distance from the origin, while for the three sector field, the distance varies according to the asymmetry values discussed above. This effect will show up later in the x-p_x history of the CR. (See Fig. 4, for example.)

In Eq. (2) above, it is assumed that the phase ϕ is zero. When this is not the case we may consider δ to be an average radial shift which is proportional to $\sin(\alpha/2)\cos\phi$ and obtain the total shift at each gap by adding the

deviation term ε, varying as $\cos(\alpha/2)\sin\phi$. Replacing δ by $\delta-\varepsilon$ at odd numbered gaps and by $\delta+\varepsilon$ at even gaps, we find an additional term in Eq. (3) so

$$x_o = -\varepsilon \sin(\nu_r\alpha/2)/\sin(\nu_r\pi/2), \qquad (2a)$$

indicating that initial x values only will be affected. (See Sec. 5.1.) Numerical agreement between Eq. (2a) and Disport-2 results is reasonable at high energies but worsens at low energies as the centering dependent phase shifts discussed below become important.

2.4 The Central Ray

Since our CR is chosen to conform with an AEO, we expect to be able to trace its characteristics back to the AEO properties just discussed. Let us begin with the $x\text{-}p_x$ history of the CR. Using $\theta_1,\theta_2,\theta_3,\theta_4,\theta_{or}$ and $\theta_{or}+\pi$ as observation points, an history of the first fifty turns is shown in Fig. 4 for four separate cases using 138^o dees in a three sector, 30 MeV proton field (E_1=143 keV/turn). The four values of θ_{or} are evenly spaced across one sector. The dots represent each of turns 1 through 5 with only every fifth turn accented for 10 through 50 for clarity. For comparison purposes we include the crosses locating AEO positions at $\theta=\theta_{or}$ and $\theta_{or}+\pi$ for appropriate energy and phase values every tenth turn starting at turn five. Qualitatively, this figure is the same as that for all other dee angles, $\phi_F(\tau)$ curves and E_1 values in a field with N=3, with the one exception of 90^o dees. In this last case, dee symmetry causes all histories to be found in the fourth ($x<0$, $p_x>0$) quadrant of the $x\text{-}p_x$ plane. Field symmetry gives this last result for all N=4 field cases.

In. Fig. 4a, the $\theta=0^o$ history is close to the line connecting the AEO positions and may be seen to begin oscillation about that line near τ=40, in accordance with the discussion of Sec. 2.1. Typical differences between CR and AEO values (e.g., $\delta x=x(CR)-x(AEO)$) are: δx=30 mils,

Figure 4.--X-P_x history of the first 50 turns for a well centered proton with $\alpha=138^{o}$, $E_f=30$ MeV, $E_1=143$ keV/turn, N=3, h=1. Every turn is given (dot) to $\tau=5$ (circled) with every fifth turn shown thereafter. Crosses mark AEO locations at 10 turn intervals beginning at $\tau=5$. All axes are in mils.

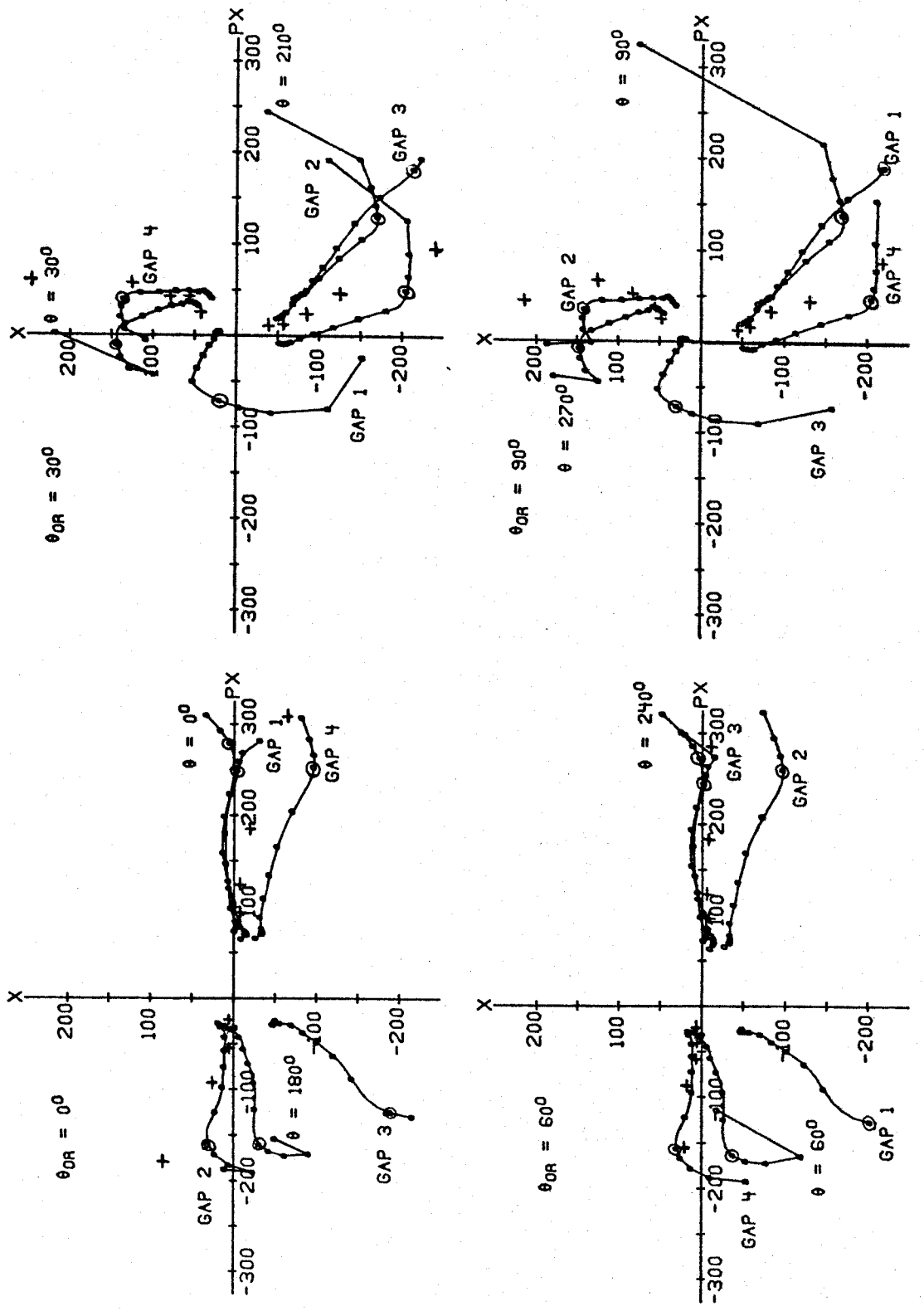
θ = 30°
θ = 210°
θ = 90°
θ = 270°
θ = 0°
θ = 180°
θ = 240°
θ = 60°
GAP 1
GAP 2
GAP 3
GAP 4
θOR = 30°
θOR = 90°
θOR = 0°
θOR = 60°
X
PX
200
100
-100
-200
-300
300

Figure 4.

δp_x=23 mils for τ=7, δx=17 mils, δp_x=-8 mils for τ=28 and δx=10 mils, δp_x=3 mils for τ=49. Starting from this history, one can easily justify the locations of the other histories by assuming that a phase point rotates counter-clockwise about the origin by an angle nearly equal to that through which the actual particle coasts between gaps and including the acceleration dependent shifts in the negative x direction at each gap.

Increasing θ_{or} from 0^o to 30^o gives Fig. 4b which may be related to Fig. 4a by reversing the roles of x and p_x. This is a direct consequence of the exchange of x and p_x asymmetry values for AEO's under the same dee rotation. These asymmetry values also account for the inequality between p_x (x) values at gaps 1 and 4 and those at gaps 2 and 3 in Fig. 4a and c (b and d). Further increments of 30^o in θ_{or} give Fig.'s 4c and d which are quite similar to Fig.'s 4a and b with a reversal in gap labels.

The second CR characteristic of interest is its phase history at each gap and the relation between these histories and $\phi_F(\tau)$. A sample set of phase histories may be found in Fig. 5a-d for the same four cases as Fig. 4a-d while the corresponding $\phi_F(\tau)$ is labeled 'C' in Fig. 17 page . There are two effects which cause deviations between $\phi_F(\tau)$ and actual CR phase histories, ϕ_{CR}. Of lesser importance is the form factor effect. In a sectored field the EO's are scalloped, a consequence of which is that the EO path

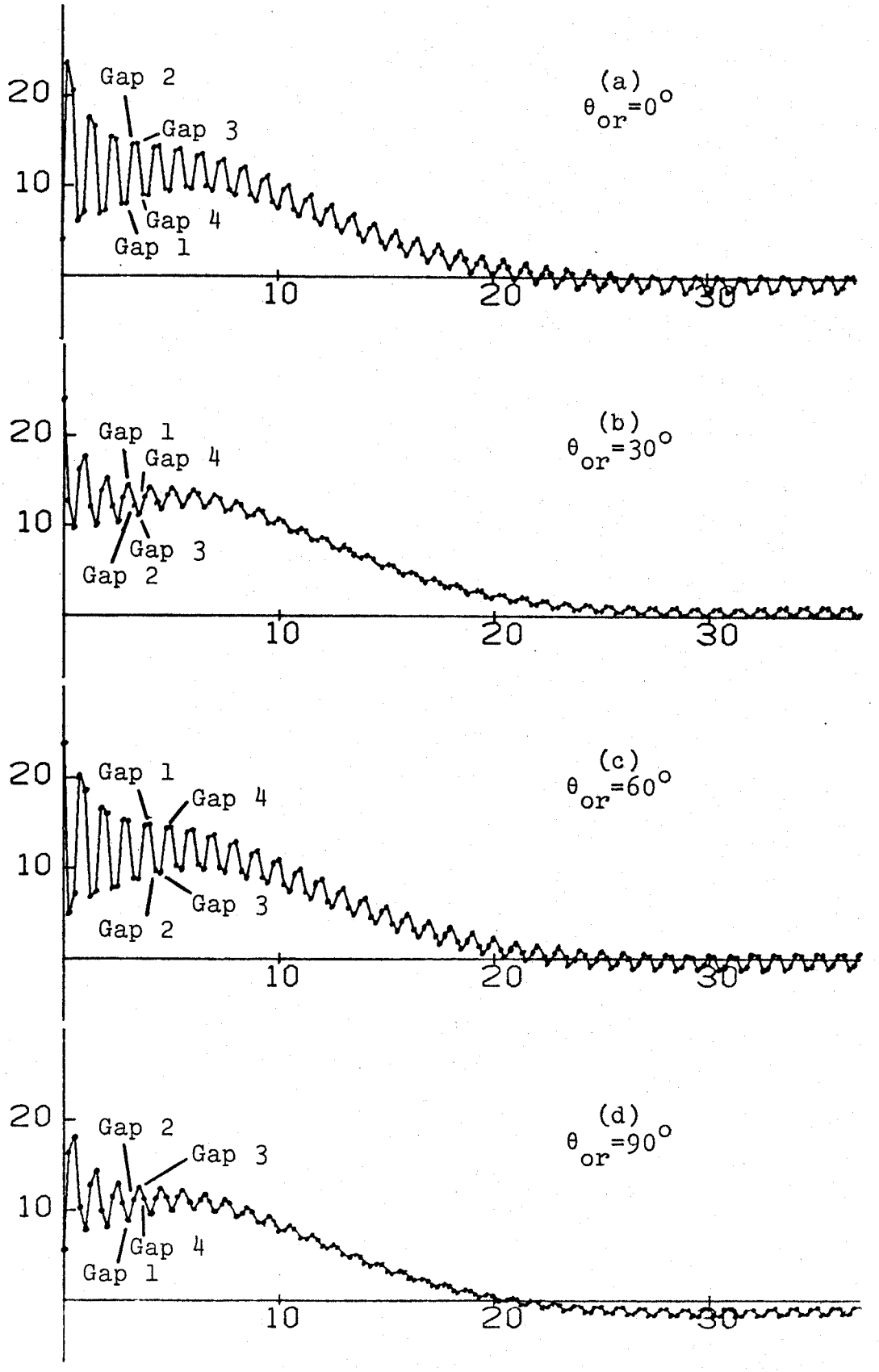

Figure 5. Phase history (deg vs. τ at each gap) for the cases shown in Fig. 4.

length is greater in the hills than in the valleys. Particle phase tends to increase while crossing hills and decrease while crossing valleys. For h=1, the phase oscillation amplitude thus produced is of the order of only one degree. This amplitude is directly proportional to h and becomes more important with higher harmonic operation.

Of greater importance are those deviations arising because the actual orbit center does not correspond to the field center, i.e., because x and p_x differ from zero. In general, one can show that the centering dependent phase shift involved with traversing an angle β may be well approximated by

$$\delta\phi_{CD} \simeq h(p_x(1-\cos\beta) + x(\sin\beta))/R_o \qquad (3)$$

where R_o should be taken as an average orbit radius and x and p_x pertain to the beginning of the angle in question. Note that $\delta\phi_{CD}$ is expected to be large only at small radii and that p_x carries the greater weighting factor if $\beta > \pi/2$ and so will usually be of greater importance than x in determining $\delta\phi_{CD}$. Since $\delta\phi_{CD}$ may easily be many degrees on early turns even for h=1, we see that there is an intimate and important connection between the centering of a particle and its phase history.

In particular, we may inspect an x-p_x history, such as Fig. 4a, and predict the $\delta\phi_{CD}$ occurring between any two dee gaps with Eq. (3). Table I contains such predictions

using reasonable R_o values for E_1=143 keV/turn and x and p_x values from Fig. 4a for the first two turns. Agreement between the quick calculation of Eq. (3) and real shifts obtained from Fig. 5a is good and may be seen to improve with energy. Because $\phi_{CR}=\phi_F$ at large τ, the larger $\delta\phi_{CD}$'s must straddle the $\phi_F(\tau)$ curve at small τ and because $\delta\phi_{CD}$ at $\theta=\theta_1$ is positive for $\theta_{or}=0^o$ we can now understand why θ_{CR} is small at $\theta=\theta_1$ and large at $\theta=\theta_2$ in Fig. 5a.

TABLE I.--Comparison of $\delta\phi_{CD}$ from Eq. (3) and $\delta\phi_{RL}$ from Fig. 5a between dee gaps i and j for $\alpha=138^o$.

τ	Gaps i	Gaps j	R_o (in.)	x (in.)	p_x (in.)	$\delta\phi_{CD}$ (deg)	$\delta\phi_{RL}$ (deg)
0	1	2	1.37	-.020	.330	23.	20.
	2	3	1.70	.010	-.190	-2.	-3.4
	3	4	1.93	-.400	-.100	-13.	-14.5
	4	1	2.17	-.075	.340	1.3	1.2
1	1	2	2.41	-.030	.280	10.8	10.7
	2	3	2.58	-.025	-.190	-1.7	-1.5
	3	4	2.76	-.310	-.120	-8.7	-9.6
	4	1	2.93	-.080	.310	.7	.4

The remaining three phase curve sets of Fig. 5 may likewise be explained using the corresponding $x\text{-}p_x$ history of Fig. 4. We take this opportunity to point out that, since the histories of Fig. 4 are qualitatively representative of all three sector field cases to be discussed below, the phase histories of Fig. 5 may likewise be considered to have all the qualitative features found in any case of interest in a three sector field.

Similar data for a four sector field is found in Fig.'s 6 and 7 respectively. Note how rapidly the crosses representing AEO's approach the origin in Fig. 6a so that only for τ=5 and 15 are they clearly visible. The cross locations are the same in Figs. 6b-d as in Fig. 6a and so are not included. The highly symmetrical AEO's give rise to very well centered beams at all dee angles, so the $\delta\phi_{CD}$'s are quite small. This implies that, in contrast to the three sector case, the relative field-dee orientation will have practically no effect on the phase histories, as inspection of Fig. 7 immediately verifies.

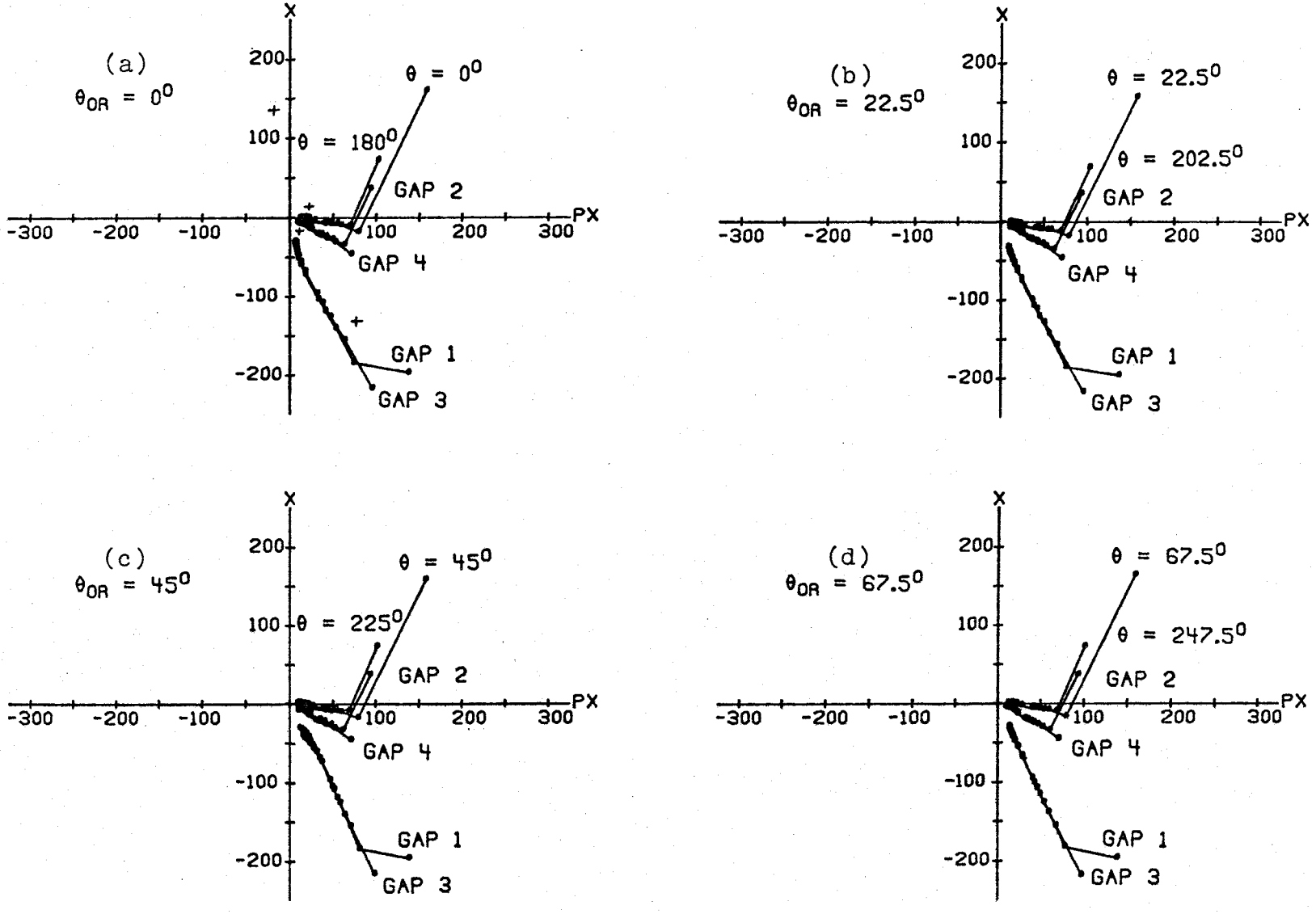

Figure 6. X-P_X history corresponding to Fig. 4 but with N=4. The first dot on each line is τ=1; excellent centering makes recognition of later turns difficult. All axes are in mils.

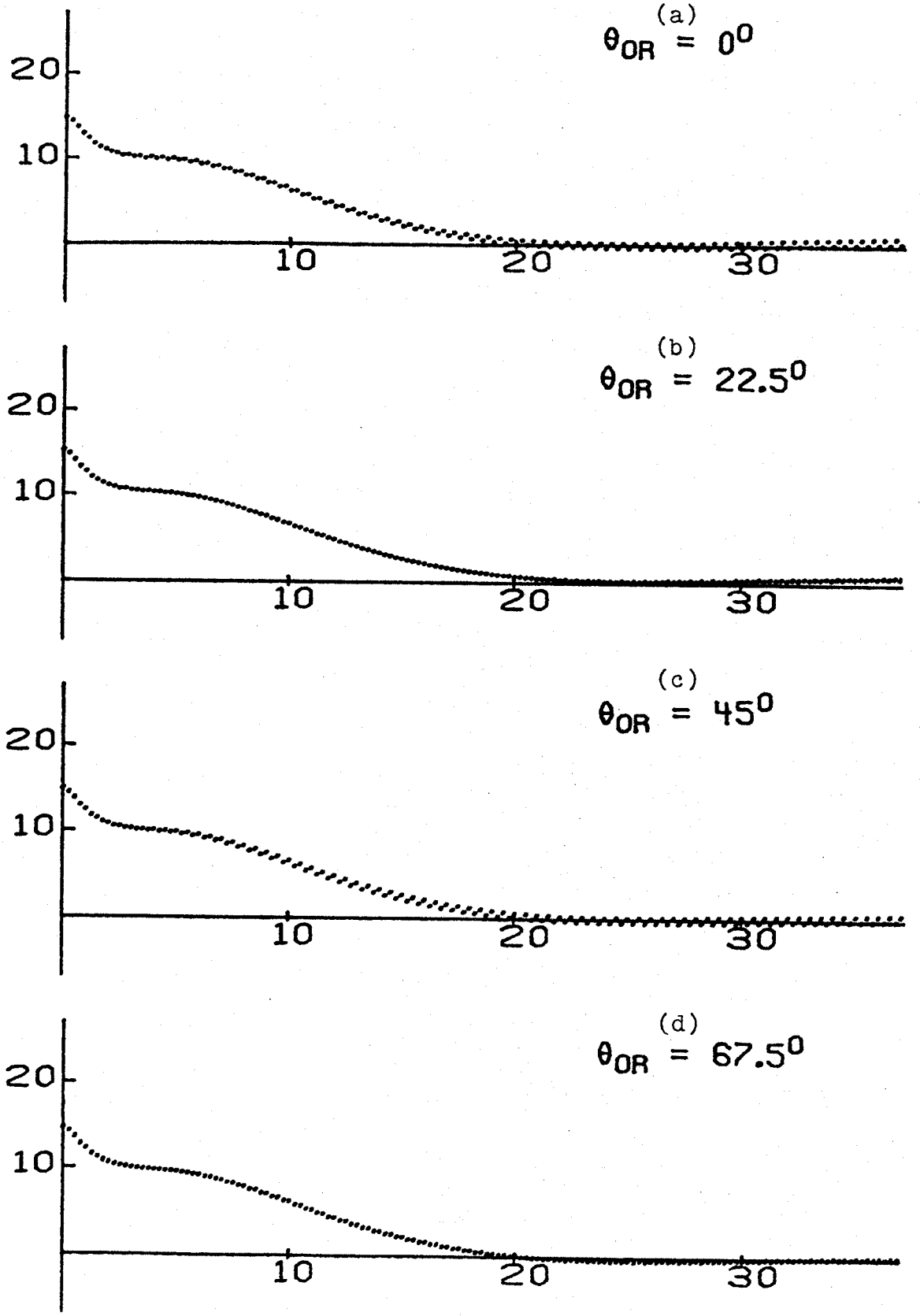

Figure 7. Phase history (deg vs. τ at each gap) for the cases shown in Fig. 6. Note that gap crossing phase is unaffected by θ_{or}, unlike in Fig. 5.

2.5 The Components of Radial Separation Between Phase Displaced Rays

Using the CR as a base, we may build up a typical beam by surrounding the CR with rays initially displaced from it in r, p_r and t. Our basic problem in analyzing phase selection is to determine, turn by turn, the radial separations of the particles constituting this beam so as to specify the most effective slit locations for eliminating those particles having phases differing from ϕ_{CR} by more than a predetermined amount. To do this we choose to resolve the radial separation, ΔR, between any two phase displaced particles, that between a particle and the CR being the most generally useful, into two components: the radial separation between the EO's having the particles' energies, and the projection on the x axis of the distance between the representative phase points on the x-p_x plane. That is,

$$\Delta R = \Delta R_{EO} + \Delta R_x. \qquad (4)$$

The first component depends only on the energy spread between the particles and is easily understood and calculated. The second component depends on a number of factors outlined later in this section and resists simple calculation. Using this decomposition, in this section we would like to lay down some general principles on how the radial separation varies with turn number and the temporal structure of the beam. We will discuss the effects of the spatial structure in the next section.

Let us start with ΔR_{EO}. It is a straight-forward job to determine that

$$R_{EO}(E,\theta) = R_o(E)(1 + F(\theta)) \tag{5}$$

describes the EO of energy E in a periodic magnetic field where

$$R_o(E) = A(2E/E_o)^{\frac{1}{2}}, \tag{6}$$

$F(\theta)$ being the orbit form factor having the same periodicity as the field.[13] This description assumes that the field is isochronous and that the energies are not relativistic. Actually, $F(\theta)$ is also a function of energy, but as long as this dependence is weak (the case in all our fields) we will suppress it, giving us a simple formula for the change in the EO with an energy change δE:

$$\Delta R_{EO}(E,\delta E,\theta) \simeq A(\delta E)(2EE_o)^{-\frac{1}{2}}(1 + F(\theta)). \tag{7}$$

A good first order approximation for the energy difference between phase displaced rays after any number of complete turns is

$$\Delta E = -E_1(\Delta\phi)\int_0^{\tau}\phi_F(\tau')d\tau' \tag{8}$$

(see Sec. 5.1.2) where $\Delta\phi$ is the initial ray phase separation. The accuracy of Eq. (8), will be tested numerically in Chapter 3. Its usefulness arises because, in conjunction with Eq. (7), it may be used as a very simple method of estimating the EO component of ΔR in Eq. (4).

The component ΔR_x in Eq. (4) does not yield to such simple calculating techniques. Let us first define this component more carefully. Consider the phase points representing the CR and a ray displaced from it in time by $\Delta\phi$ but of equal energy. Let us label these rays C and D, respectively. We will find it convenient to define the vector Λ in the $x\text{-}p_x$ plane between the points representing such particles. The components of Λ are

$$\lambda_x = x_D - x_C,$$

$$\lambda_p = p_{xD} - p_{xC},$$

while its length is

$$\lambda = (\lambda_x^2 + \lambda_p^2)^{\frac{1}{2}}.$$

As defined above, λ_x is equivalent to the ΔR_x of Eq. (4) and will be used in place of the latter from now on.

We now examine the processes affecting Λ and, in particular, its length λ. Let us start with C and D lying on the same x, p_x point. We assume that their energy is small compared with E_f and that $|\nu_r - 1| \simeq 0$. Figure 8a shows this initial situation. At the first acceleration gap, the energy increase δE produces a sudden jump in R_{EO} which appears as a discontinuous shift by the phase points in the negative x direction of magnitude δR_{EO} given by Eq. (7). (See Fig. 8a). (We shall neglect the small concommittant changes in P_{REO}.) The points will then be separated along the x axis by a distance given by Eq. (7), where δE is taken as the

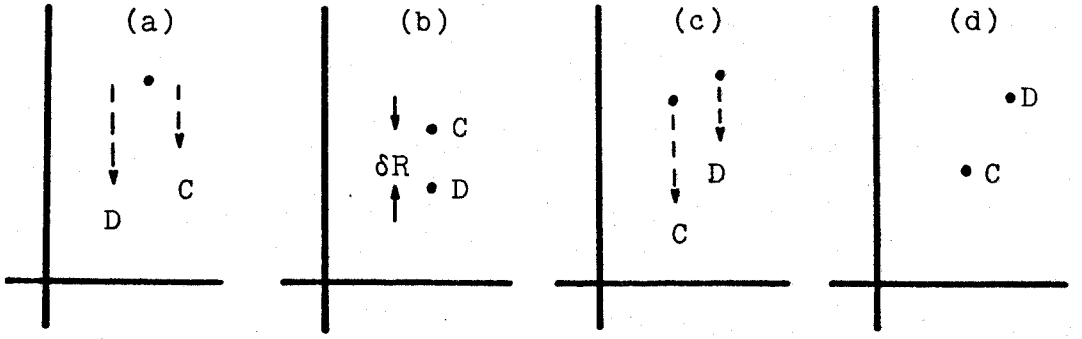

Figure 8. Schematic representation of the growth of Λ between the CR (point C) and a phase displaced ray (point D). (See text, p. 37.)

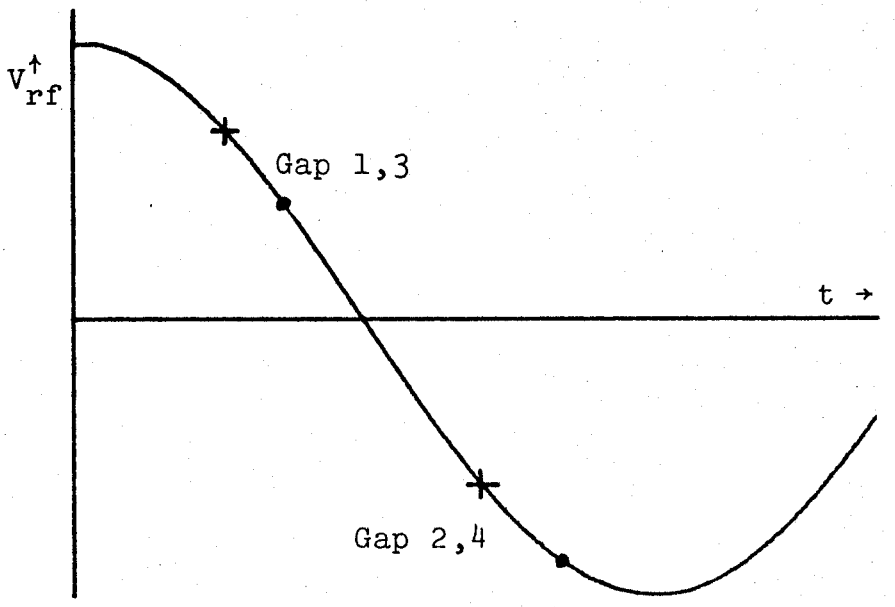

Figure 9. Difference in rf times of gap crossings for zero (crosses) and non-zero (dots) phases for h=1.

difference in energy gains between the particles, ΔE_G. (Figure 8b.) We term this process "disjunction". During the drift between gaps, θ, Λ rotates counterclockwise about its origin by the angle $\nu_r\theta$ (Fig. 8c.). At each succeeding gap, Λ undergoes a change in length, $\delta\lambda$, which depends on ΔE_G and the orientation of Λ, since only λ_x changes in the disjunction process (Fig. 8d).

Further insight into this process may be obtained by considering the net disjunction from a pair of opposite gaps. For $\alpha=180^o$ and $\nu_r\simeq 1$, $\Delta\Lambda$ over one turn is parallel to the x-axis with magnitude given by the difference between the $\delta\lambda$'s at each gap because $\nu_r\theta$ should increase by nearly 180^o between such gaps. (This assumes that $\Delta E_G = \delta E(\Delta\phi)-\delta E(CR)$ has the same sign at both gaps, the usual case.) This difference is zero under only the most extra-ordinary circumstances since $\delta\lambda$ depends on energy and phase by Eq.'s (7) and (8) while the same half turn asymmetry discussed in connection with AEO's modifies the $\delta\lambda$ of the first gap when seen at the opposite gap in a three sector field.

With four accelerating gaps, the net disjunction is quite different for the second gap pair, $\Delta\lambda_{24}$, than for the first, $\Delta\lambda_{13}$. Most apparent is the difference in the actual rf times of gap crossing involved for a constant non-zero phase. Figure 9 shows such times for some (arbitrary) values of α and ϕ_{CR} (dots) on a part of an rf wave, along with the corresponding zero phase times (crosses). Vertical distance

between the dot and cross for a given gap translates directly into a difference in disjunctive effects between gap pairs. We shall term this the rf asymmetry effect.

Furthermore, in any four gap situation, the net change in Λ over one turn as measured at $\theta=\theta_{or}$, for example, is

$$\Delta\Lambda = (\Delta\lambda_{13})K_1 + (\Delta\lambda_{24})K_2. \qquad (9)$$

The K_1 and K_2 are vectors depending on the dee angle since, to first order, they would parallel the respective gap pairs. But K_1 and K_2 are not simple to calculate accurately since they also depend on the past acceleration history of Λ. The disjunction at an intervening gap effectively changes the angle of rotation of Λ from the expected value of nearly 180^{o} between opposing gaps, a change which must be reflected in K_1 and K_2. We shall refer to Eq. (9), linking the net disjunctions at each pair of opposing gaps to the change in Λ per turn, as defining the gap-pair coupling effect.

We now can see that it would be quite difficult to calculate this second component of ΔR. To obtain an expression like Eq. (5) for λ or Eq. (7) for $\Delta\lambda$, one would need an analytical form for the phase as a function of gap and turn numbers, which is not readily available ($\phi_F(\tau)$ is absolutely inadequate for this), and a similar form for the vectors K_1 and K_2 in Eq. (9) above.

In lieu of the optimal situation, we present Fig. 10 showing the x-p_x history over the first 40 turns at $\theta=0^o$ for two rays separated by $\Delta\phi=\pm 2^o$ from the CR, used as the origin of the figure. This CR is the ray, the x-p_x and phase histories of which were used in Fig.'s 4a and 5a. Note that precession becomes apparent near turn 6 or 7 where $\nu_r \simeq 1.01$, that λ becomes constant at about 11 mils after 10 or so turns, where $\nu_r \simeq 1.02$, and that only precession is important thereafter.

From a broader viewpoint, the process whereby Λ increases in length may be seen as a resonance phenomenon driven by the asymmetries present in the acceleration process. In both three and four sector fields, if $\phi_F(\tau)$ alone were accurate at each gap of turn τ, a driving asymmetry would be present since the first derivatives of the rf waveform yielding $\Delta E_G (\simeq (\Delta\phi/\omega_{rf})(dV_{rf}/dt))$ would be different at each gap crossing (see Fig. 9, for example) so the $\delta\lambda$'s from different gaps would rarely cancel (the rf symmetry effect). The centering dependent phase shift which actually always occurs serves to accentuate this asymmetry in almost all cases since $\phi_F(\tau)$ is large where $\delta\phi_{CD}$ is large. (Exceptions to be noted later occur when the phase at gaps 2 and/or 4 exceeds $(\pi-\alpha)/2$.) In three sector fields, there is an additional driving asymmetry represented by the gap-crossing resonance discussed in connection with the AEO. As will be shown clearly by data below, λ shows

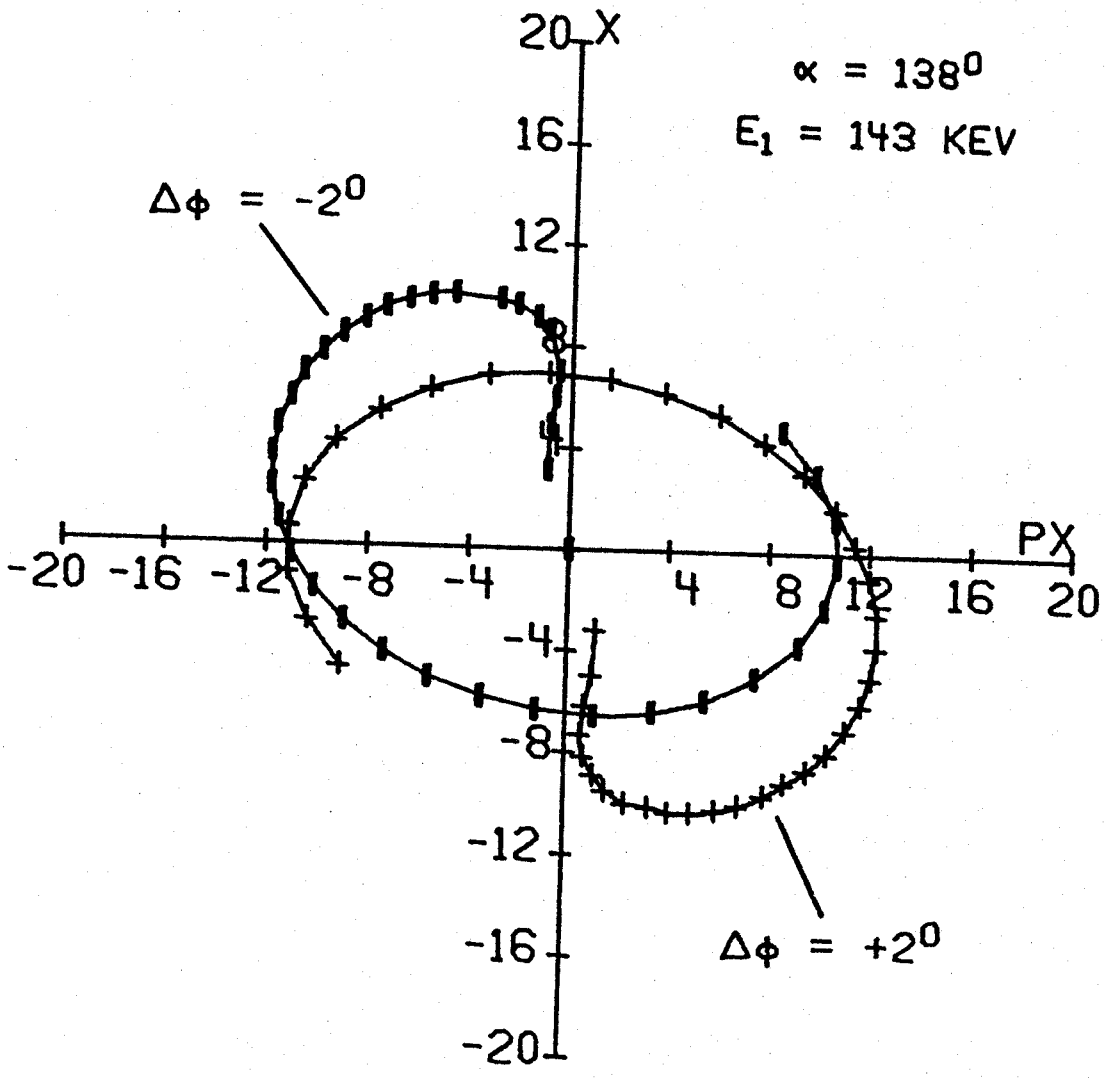

Figure 10. δx-δp_x history for the first 40 turns for rays with $\Delta\phi=\pm 2^{\circ}$. Properties of the reference CR are shown in Figs. 4a and 5a. Points are plotted once per turn at $\theta=\theta_{or}=0^{\circ}$. All axes are in mils.

much larger variations with changing acceleration parameters in three sector fields than in four sector fields because of this second driving term. A decrease in the rate of resonant growth of Λ occurs as ϕ_{CR} approaches $\phi_F(\tau)$ which in turn approaches zero, as the energy in the denominator of Eq. (7) becomes large and as $\nu_r - 1$ begins to deviate significantly from zero. It is this last condition which really destroys the resonance regardless of the influence of the first two.

We have now seen that both ΔR_{EO} and λ depend on the ray phase separation $\Delta\phi$, ΔR_{EO} through Eq.'s (7) and (8) and λ through a more circuitous route involving the disjunction process. Discussion of phase selection and the evaluation of parameter effects may be facilitated by introducing a quality factor Q as

$$Q = Q_{EO} + Q_x = (\Delta R)/(\Delta\phi), \tag{10}$$

where

$$Q_{EO} = (\Delta R_{EO})/(\Delta\phi),$$

$$Q_x = \lambda_x/(\Delta\phi).$$

Note that, although we do not show it explicitly, Q is a function of τ and θ. Obviously, large Q implies good phase selection. It is the behavior of Q with τ, θ and various machine parameters which we shall actually be investigating in the next chapter.

We shall regard Q as constant with respect to $\Delta\phi$ in any given situation. Orbit calculations show that, for most cases below, this is true for $\Delta\phi$ as large as 32^{o}. Even for the exceptional cases, Q may easily be assumed to be constant over the small $\Delta\phi$ we would expect a practical slit to pass.

2.6 Effects of Radial Emittance

We now turn to the consequences of having sources of finite width emitting particles in many directions. The most important mechanism to be considered is the centering dependent phase shift of Eq. (3) which imparts a time displacement relative to the CR, $\delta\phi$, depending on the initial particle position in the δx-δp_x plane $(\delta x_o, \delta p_{xo})$ having the CR as origin. On early turns, R_o increases rather rapidly, even on a single turn, so that an average phase shift $\delta\phi_{av}$ develops between a spatially displayed ray and the CR. Consider the five rays labeled A through E in Fig. 11a at $\tau=0$. Their subsequent phase behavior relative to the CR appears in Fig. 12. Again, the CR is that used in Fig.'s 4a, 5a and 10. Note that the rays of larger δp_{xo} tend to develop the larger $\delta\phi_{av}$'s. Note also that there is a small amplitude ($\sim 0.1^o$ compared with $\sim 1.1^o$ average shift) phase oscillation appearing at larger turn numbers where R_o varies only slowly. The phase oscillations are related to the slow oscillation of the displaced ray about the CR, particularly the changing δp_x values.

Figure 11 may be taken as showing the evolution of a section of phase space assumed occupied by beam at 5 turn intervals from its initial circular condition at $\tau=0$ to $\tau=25$

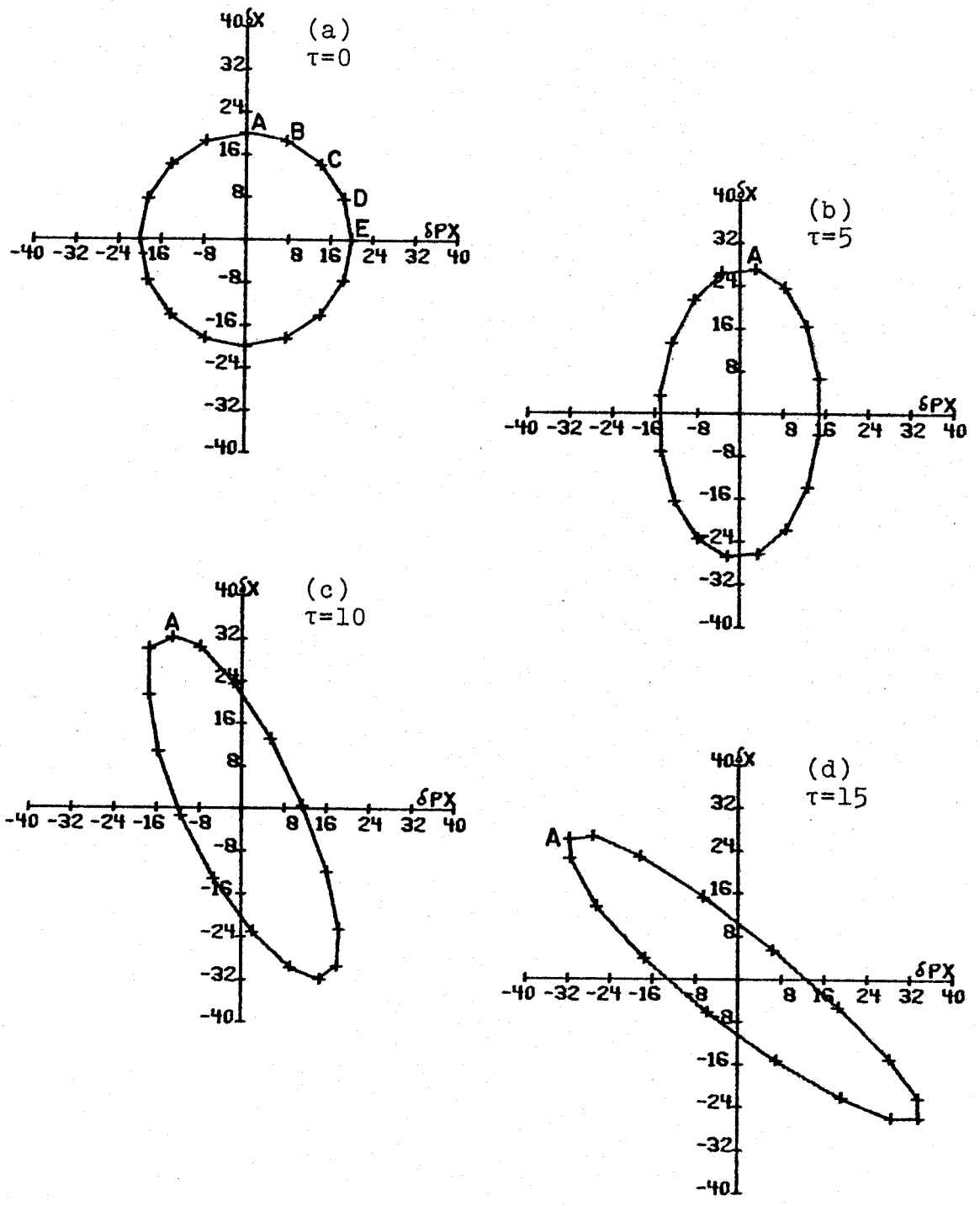

Figure 11. δx-δp_x history for 16 rays initially located on a circle of 20 mil radius. Properties of the reference CR are shown in Figs. 4a and 5a. All axes are in mils.

Fig. 11. Cont.

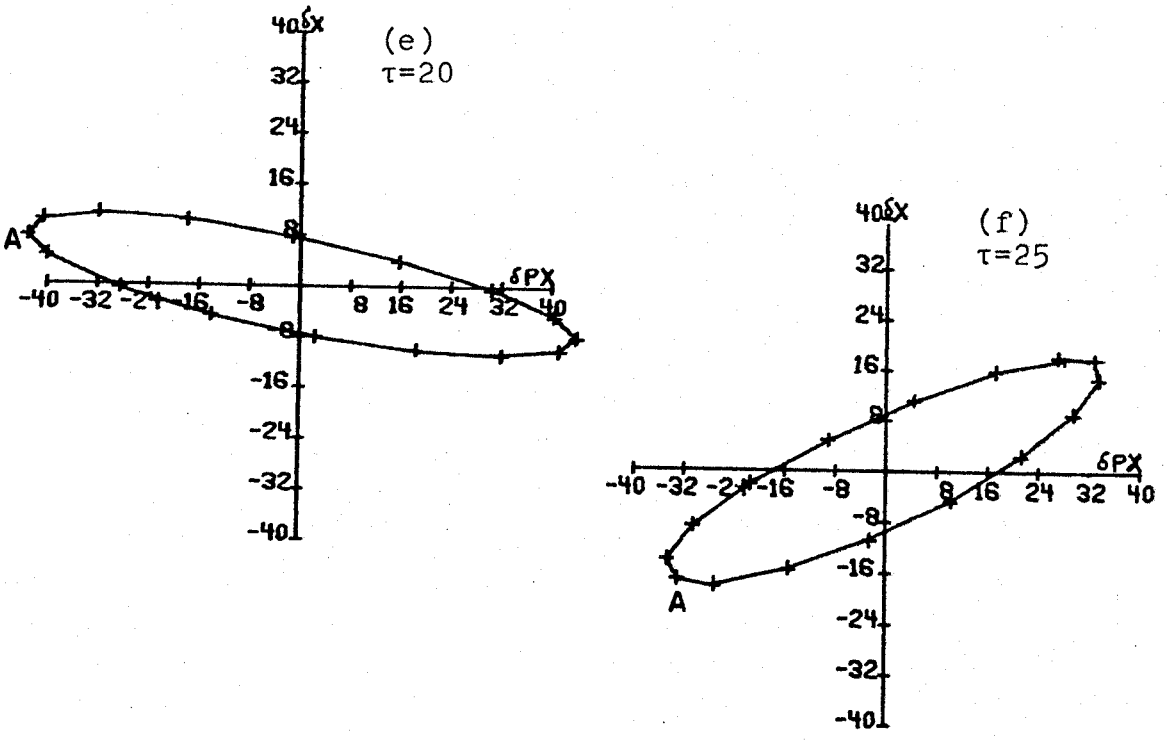

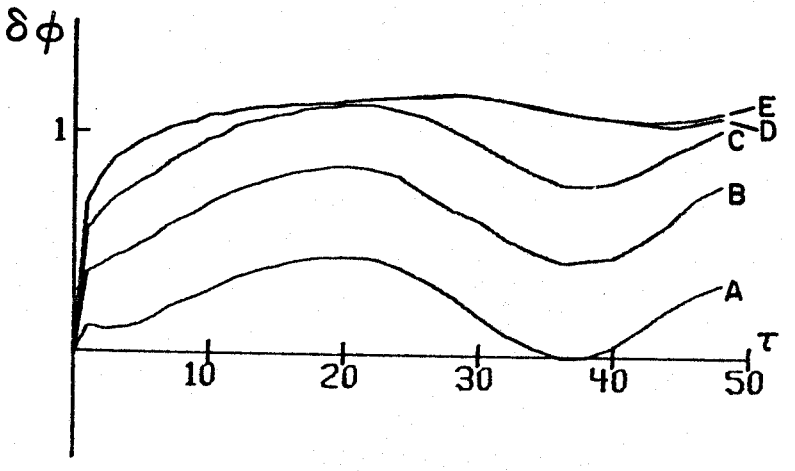

Figure 12. δφ(deg) relatice to the CR vs. τ for rays with the initial spatial displacements shown by the correspondingly labeled points in Fig. 11a.

(Fig. 1f). The distortion of the original (arbitrary) circular shape may be seen to be essentially complete by τ=15 and the resultant beam ellipse mainly rotates thereafter. A nice explanation of this phenomenon has been given by Bolduc and Mackenzie.[14] The occupied area on the δx-δp_x plane varies from 1256 mils^2 at τ=0 to nearly 1200 mils^2 at τ=15, a pleasing result since the accompanying δE-$\delta\phi$ co-ordinate changes are small.

There is a fixed relationship between the orientation of the ellipses in Fig. 11 and the phase oscillations of Fig. 12 such that, for a given ray, the turn where its extreme δp_x value occurs corresponds to the turn with an extremum in its $\delta\phi$. Finally, note that, just as the rays of larger δx_o experience larger distortions in the δx-δp_x plane, so do they also show larger oscillations about their $\delta\phi_{av}$ (~0.3° with ~0.3° average shift).

While we will emphasize the effects of temporal over spatial displacements in this paper, we will present some data pertinent to the behavior of rays with the initial conditions used above for Fig. 11. We should, therefore, establish whether the effects we see are linear with δx_o and δp_{xo}. Figure 13 gives values of $(\delta x^2 + \delta p_x^2)^{\frac{1}{2}}$ between the CR and the ray marked 'A' in Fig. 11 as functions of initial δx_o and δp_{xo} for three different dee angles. For values of 150 to 200 mils one observes deviations from linearity, especially for 90° dees, but for smaller values

Figure 13.--$(\delta x^2+\delta p_x^2)^{1/2}$ vs. δx_o and δp_{xo} at various dee angles. Variation is close to linear over the range of initial conditions shown for all dee angles.

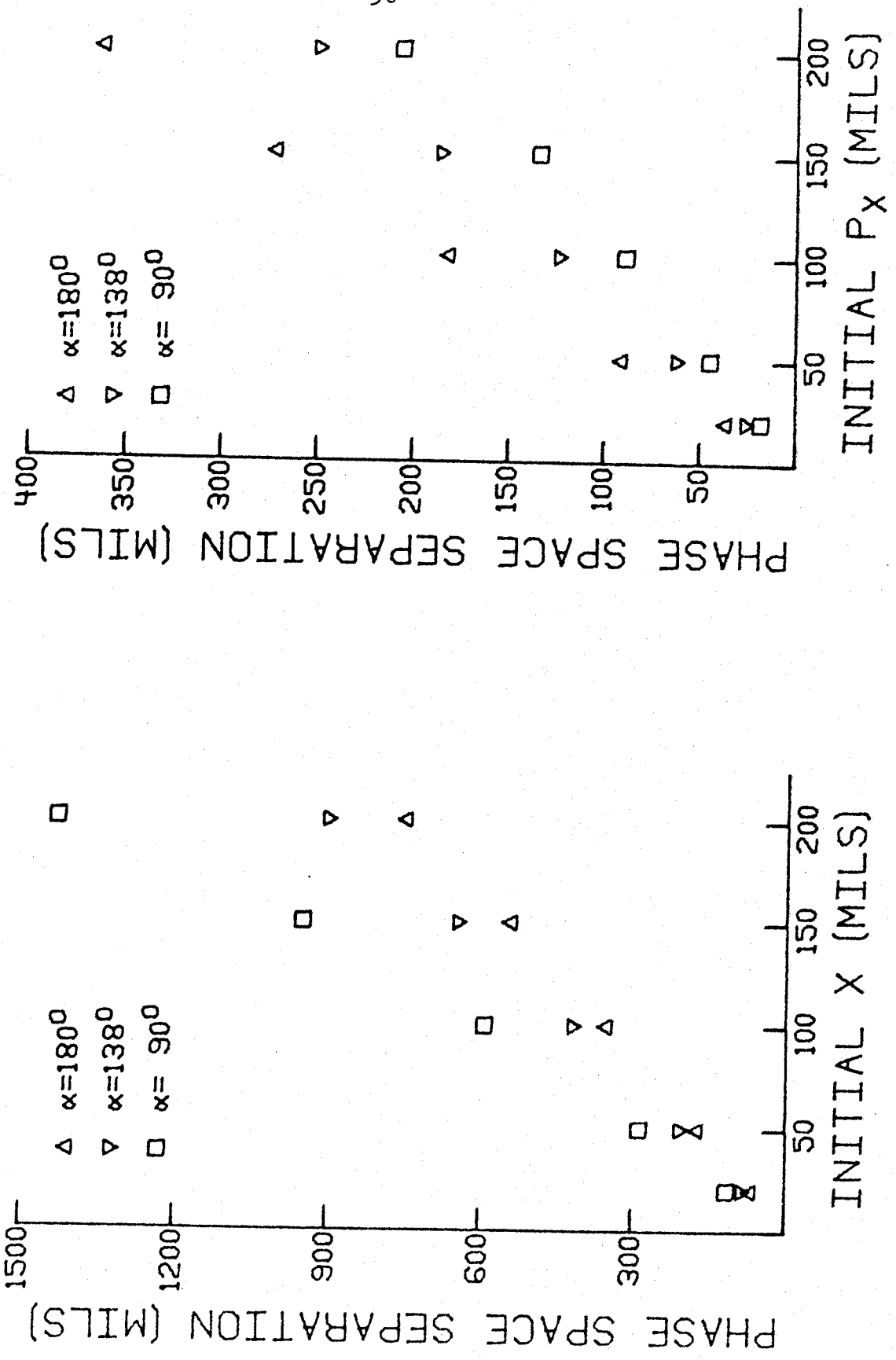
PHASE SPACE SEPARATION (MILS)
400
350
300
250
200
150
100
50
50
100
150
200
INITIAL P_X (MILS)
α=180°
α=138°
α= 90°
PHASE SPACE SEPARATION (MILS)
1500
1200
900
600
300
50
100
150
200
INITIAL X (MILS)
α=180°
α=138°
α= 90°

Figure 13.

corresponding more closely with the δx-δp_x areas to be expected in a high resolution cyclotron, any deviations are unnoticable.

While it does not affect our discussion, one should note that δx and δp_x related phenomena are not generally linear as emphasized in Fig. 4 of the work of Blosser previously cited.[5]

As the data in Fig. 13 implies, the $\delta\phi_{av}$ are, however, found to vary quite linearly with both δx_o and δp_{xo} in the range used. Table II gives approximate rates of increase of $\delta\phi_{av}$ with δx_o and δp_{xo} observed on turn 20 with $\alpha=138^o$ ($\alpha=90^o$ for h=3) on acceleration harmonics h=1, 2 and 3. The $\delta\phi_{av}$ for the δp_{xo} displaced rays grow at better than twice the rate for the δx_o displaced rays on all harmonics. That $\delta\phi_{av}$ shows unexpected behavior for h=2 has to do with precisely how the $\delta\phi_{av}$ is generated and is not germane to our purpose.

TABLE II.--Rate of increase of $\delta\phi_{av}$ and δx_o and δp_{xo} in (deg/10 mils) at $\tau=20$.

	h=1	h=2	h=3
δx_o	.22	.10	.45
δp_{xo}	.56	.50	1.40

Since $\delta\phi_{av}$ as a function of τ increases from zero at $\tau=0$ while $\phi_F(\tau)$ decreases from its maximum at that point, from Eqs. (7) and (8) it is not surprising that the rays

under discussion show very small ΔR_{EO} values. In fact, the rate of increase of ΔR_{EO} with δx_o and δp_{xo} is about an order of magnitude less than that shown in Fig. 13 for the increase in phase space displacement.

We make these comments by way of explaining that the radial separation between the CR and spatially displaced rays is insensitive to the parameters in Chapter 3 except for h, the effect of which is summarized in Table II. Therefore, we present no further data on such rays in Chapter 3. We will, however, return to this subject when the question of locating phase selective slits arises in Chapter 4.

3. DATA AND ANALYSIS

Without exception, the data quoted for ΔR_{EO}, λ and λ_x in tables in this chapter are values measured between two rays initially displaced by $\Delta\phi=\pm 2^o$ from the CR. Therefore, using the appropriately labeled columns in any table, one can obtain the Q values as defined in Eq. (10) from $Q_{EO}=\Delta R_{EO}/4$ and $Q_x=\lambda_x/4$. To minimize the number of minus signs used, the table entry ΔR_{EO} is taken as positive if $\Delta R_{EO}\ (-2^o)>\Delta R_{EO}(+2^o)$, the usual case for a positive phase curve. Likewise, the table entry λ_x is positive if $\lambda_x(-2^o)>\lambda_x(+2^o)$.

3.1 Dee Angle and Orientation

In this section we wish to discover how the dee angle (α) and orientation (θ_{or}) affect ΔR corresponding to an initial $\Delta\phi$. All results in this section were obtained from Devil using a three sector proton field with E_f=30 MeV, E_1=143 keV/turn and the $\phi_F(\tau)$ curve labeled "C" in Fig. 17.

Figure 14 gives, as functions of energy, the eigen-ellipse axis length ratios and the flutter, here calculated as $H_3(r)/\langle B(r)\rangle$ where $H_3(r)$ is the co-efficient of $\cos(3\theta)$ and $\langle B(r)\rangle$ is the θ independent term in the Fourier representation of the field ($\theta=0^o$ is a valley center). Figure 15 contains ν_r and the peak energy gain precession angle

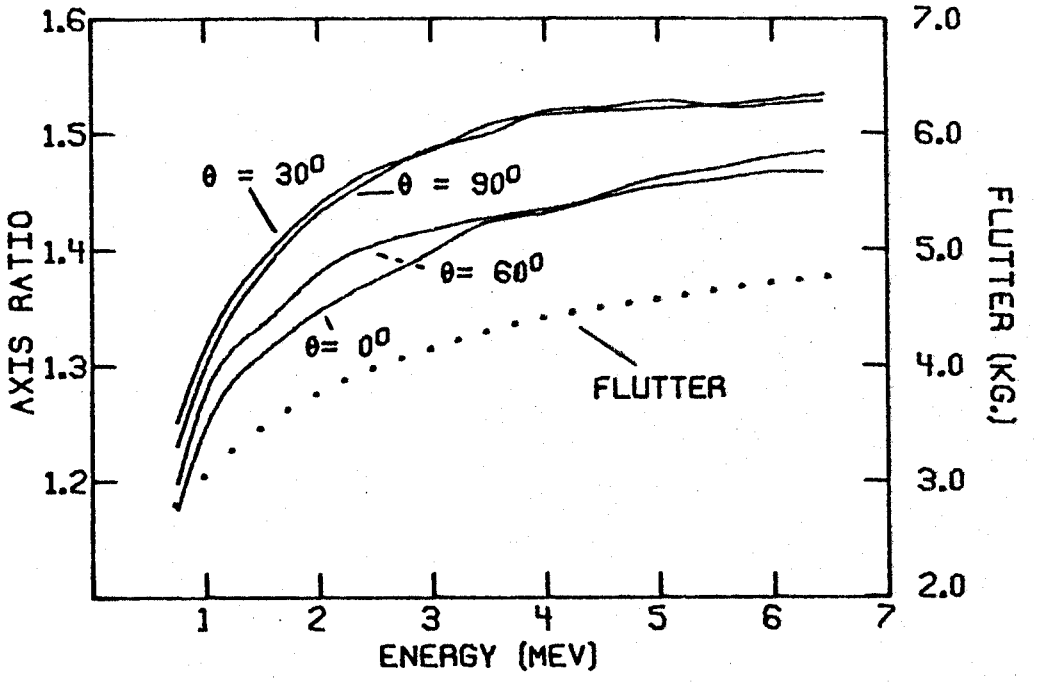

Figure 14. Eigen-ellipse axis length ratios and flutter vs. energy for an M.S.U. proton field with N=3, E_f=30 MeV.

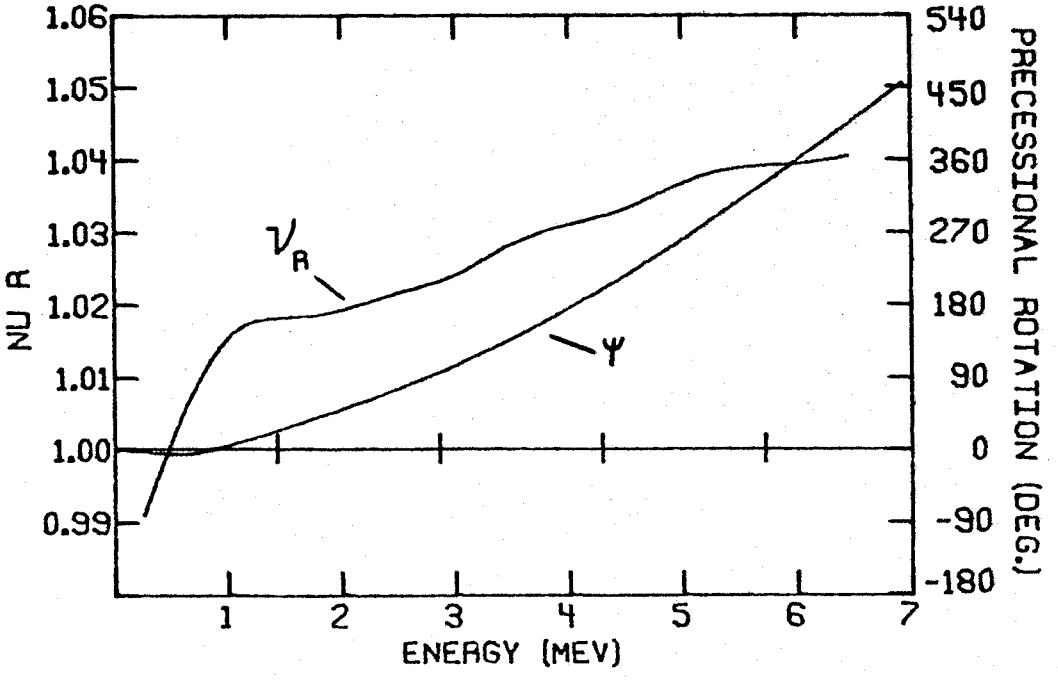

Figure 15. ν_r and ψ(see Eq. 11) vs. energy for the field of Fig. 14.

$$\psi = (2\pi/E_1)\int_0^E (\nu_r - 1)\, dE', \qquad (11)$$

also plotted against energy. Both figures are presented for future reference. Four sector field results will be discussed separately in Sec. 3.5.

In the tables appearing below, the θ_{or} values used are evenly spaced throughout one sector while the labels "H" and "V" are used to indicate a hill or valley center where appropriate.

Let us first examine the radial separation component given by Eqs. (7) and (8) to both assure the accuracy of these equations and determine the effects of α and θ_{or}. Table III gives ΔE and ΔR_{EO} for four values of θ_{or}. Turn 14 entries are included because $\Delta R_{EO}(\tau=14)$ is the maximum value for the chosen $\phi_F(\tau)$ curve while turn 21 entries are present because $\phi_F(\tau=21)\simeq 0^o$. If one compares the ΔE values in the table with the values found using $\phi_F(\tau)$ and Eq. (8) of $\Delta E(\tau=14)=28$ keV and $\Delta E(\tau=21)=30$ keV one finds a variation of ΔE with θ_{or} mirroring the form factor phase shift. This shift corresponds to crossing half a valley for $\theta_{or}=30^o$ or half a hill for $\theta_{or}=90^o$ and is present because ϕ_{CR} was forced to be 0^o at θ_{or} at the same large turn number in all cases. The ΔE's from Eq. (8) are slightly higher than the values at $\theta_{or}=0^o$ because the $\delta\phi_{CD}$ values tend to

TABLE III.--ΔE and ΔR_{EO} at $\theta=\theta_{or}$ and $\theta=\theta_{or}+\pi$ for various dee angles. The magnetic field used corresponds to curve C in Fig. 17.

N=3 h=1 E_1=143 keV/turn $\Delta\phi=\pm2^{o}$

τ	θ_{or}	α=180 ΔE (keV)	α=180 ΔR_{EO} (mils)	α=150 ΔE (keV)	α=150 ΔR_{EO} (mils)	α=138 ΔE (keV)	α=138 ΔR_{EO} (mils)	α=120 ΔE (keV)	α=120 ΔR_{EO} (mils)	α=90 ΔE (keV)	α=90 ΔR_{EO} (mils)
14	0.(V)	25.	43.	25.	45.	25.	45.	25.	44.	23.	40.
	180.(H)	26.	49.	26.	51.	26.	51.	25.	50.	24.	46.
	30.	28.	52.	27.	51.	27.	51.	27.	49.	27.	50.
	210.	29.	53.	28.	52.	28.	52.	28.	52.	27.	51.
	60.(H)	26.	51.	24.	49.	24.	49.	24.	49.	25.	50.
	240.(V)	26.	45.	25.	44.	25.	44.	25.	44.	26.	44.
	90.	23.	43.	23.	44.	23.	44.	23.	44.	22.	41.
	270.	24.	42.	24.	44.	24.	44.	24.	43.	22.	41.
21	0.(V)	28.	39.	29.	42.	29.	41.	28.	41.	26.	37.
	180.(H)	28.	44.	29.	47.	29.	47.	28.	46.	26.	43.
	30.	32.	49.	32.	48.	32.	48.	32.	49.	32.	48.
	210.	33.	49.	32.	49.	32.	49.	32.	50.	32.	48.
	60.(H)	29.	47.	28.	46.	28.	46.	28.	46.	29.	47.
	240.(V)	29.	41.	28.	40.	28.	40.	28.	41.	29.	41.
	90.	25.	38.	26.	40.	26.	40.	26.	40.	24.	38.
	270.	25.	37.	26.	39.	26.	39.	26.	39.	25.	37.

push the average of $\phi_{CR}(\tau)$ below $\phi_F(\tau)$ on early turns. Note that the ΔR_{EO}'s vary as the corresponding ΔE's, but modified by $F(\theta)$. The 13% variation between hill and valley values of ΔR_{EO} may be calculated using the field flutter; comparing τ=14 and τ=21 data shows this variation to be independent of energy, at least in this small region of interest. In summary, our data show that dee angle is of rather little consequence in determining ΔR_{EO}, but that θ_{or} is of definite importance.

Table IV lists λ and λ_x values. At this point we will explain only the qualitative details of the λ data by using the appropriate ϕ_{CR}, exemplified in Fig. 5. We shall return to the λ_x values in Chapter 4.

The simplest case to discuss is, of course, $\alpha=180^o$ where there is no gap pair interaction (cf. Eq. (9)), where positive phase always means that $\delta\lambda(=\Delta R_{EO}(+\Delta\phi)-\Delta R_{EO}(-\Delta\phi))<0$ at each gap and where, on early turns, $\lambda_x=\lambda$. The net $\Delta\Lambda$ per turn will depend on the difference in ΔE's between the gaps and should, therefore, vary roughly as the area between the phase histories at the two gaps. However, when E is small, the $(E)^{-\frac{1}{2}}$ dependence of Eq. (7) must be considered, so that the question of whether the larger phase (and, hence, ΔE) occurs at θ_1 or θ_2 becomes important. With regard to achieving large final λ's, the area dependence favors $\theta_{or}=0^o,60^o$ while the energy favors $\theta_{or}=30^o,60^o$, adding to a double blessing on $\theta_{or}=60^o$ and a double curse on $\theta_{or}=90^o$.

TABLE IV.--λ and λ_x at $\theta=\theta_{or}$ and $\theta=\theta_{or}+\pi$ for the same cases as shown in Table III.

N=3 h=1 E_1=143 keV/turn $\Delta\phi=\pm2^\circ$

τ	θ_{or}	α=180 λ (mils)	α=180 λ_x (mils)	α=150 λ (mils)	α=150 λ_x (mils)	α=138 λ (mils)	α=138 λ_x (mils)	α=120 λ (mils)	α=120 λ_x (mils)	α=90 λ (mils)	α=90 λ_x (mils)
14	0.	34.	-23.	36.	-26.	24.	-19.	7.	-6.	49.	14.
	180.	34.	29.	35.	30.	23.	20.	4.	3.	43.	-24.
	30.	25.	20.	33.	30.	31.	28.	29.	28.	20.	12.
	210.	35.	-23.	49.	-37.	47.	-36.	46.	-44.	34.	-22.
	60.	53.	46.	76.	68.	74.	67.	77.	70.	60.	56.
	240.	53.	-34.	75.	-53.	73.	-53.	76.	-56.	58.	-47.
	90.	16.	-12.	9.	-6.	4.	3.	29.	21.	81.	56.
	270.	11.	9.	5.	2.	6.	-6.	24.	-22.	61.	-52.
21.	0.	37.	-3.	38.	-7.	25.	-7.	10.	-10.	58.	-22.
	180.	26.	6.	25.	2.	17.	4.	10.	10.	49.	30.
	30.	28.	-5.	36.	0.	34.	-2.	34.	-6.	31.	-18.
	210.	24.	2.	37.	-7.	34.	-5.	31.	-2.	18.	11.
	60.	40.	1.	57.	11.	55.	12.	56.	14.	42.	18.
	240.	56.	0.	80.	-8.	77.	-9.	79.	-11.	57.	-16.
	90.	11.	-1.	4.	1.	8.	4.	30.	9.	73.	16.
	270.	12.	-3.	77.	-5.	7.	-5.	26.	-5.	70.	-2.

If one studies data at fixed θ_{or} for decreasing α, one observes systematic changes as gap pair interactions take precedence. Among these is a rather subtle interaction, not previously mentioned, between the magnetic field sector structure represented by the eigen-ellipse and the gap pair interaction which produces the early turn orientation of Λ on the x-p_x plane. First of all, the eigen-ellipse major axis rotates as one continuously changes his observation angle θ so that it forms an angle with the positive p_x axis of $\theta_e(\theta)$ which, for N=3, at $\theta=0^o,30^o,60^o,90^o$ is given by $\theta_e=0^o,45^o,90^o,135^o$. Since for N=3, $\theta_e(\theta)$ is periodic over 120^o, upon traversing 180^o of azimuth, one finds the eigen-ellipse "rotated" by 90^o. (Recalling our comments on the AEO's in the same type of field, it becomes apparent that the eigen-ellipse gives us an easily visualized method of determining orbit asymmetry effects.) Now, when Λ is parallel to the eigen-ellipse major axis, λ will be maximum (note the $\theta_{or}=30^o$, $\theta=210^o$ and $\theta_{or}=90^o$, $\theta=90^o$ entries in Table IV), and when Λ parallels the minor axis, λ will be minimum ($\theta_{or}=30^o$, $\theta=30^o$ and $\theta_{or}=90^o$, $\theta=270^o$).

Certainly a much more graphic demonstration of this phenomenon is found in the oscillations of the curves of λ as a function of τ in Fig. 16. The data in Table IV for $\alpha=138^o$ represents two points on these curves for each θ_{or} value. The oscillation amplitude is determined by the requirement that the extreme values be in the ratio of the

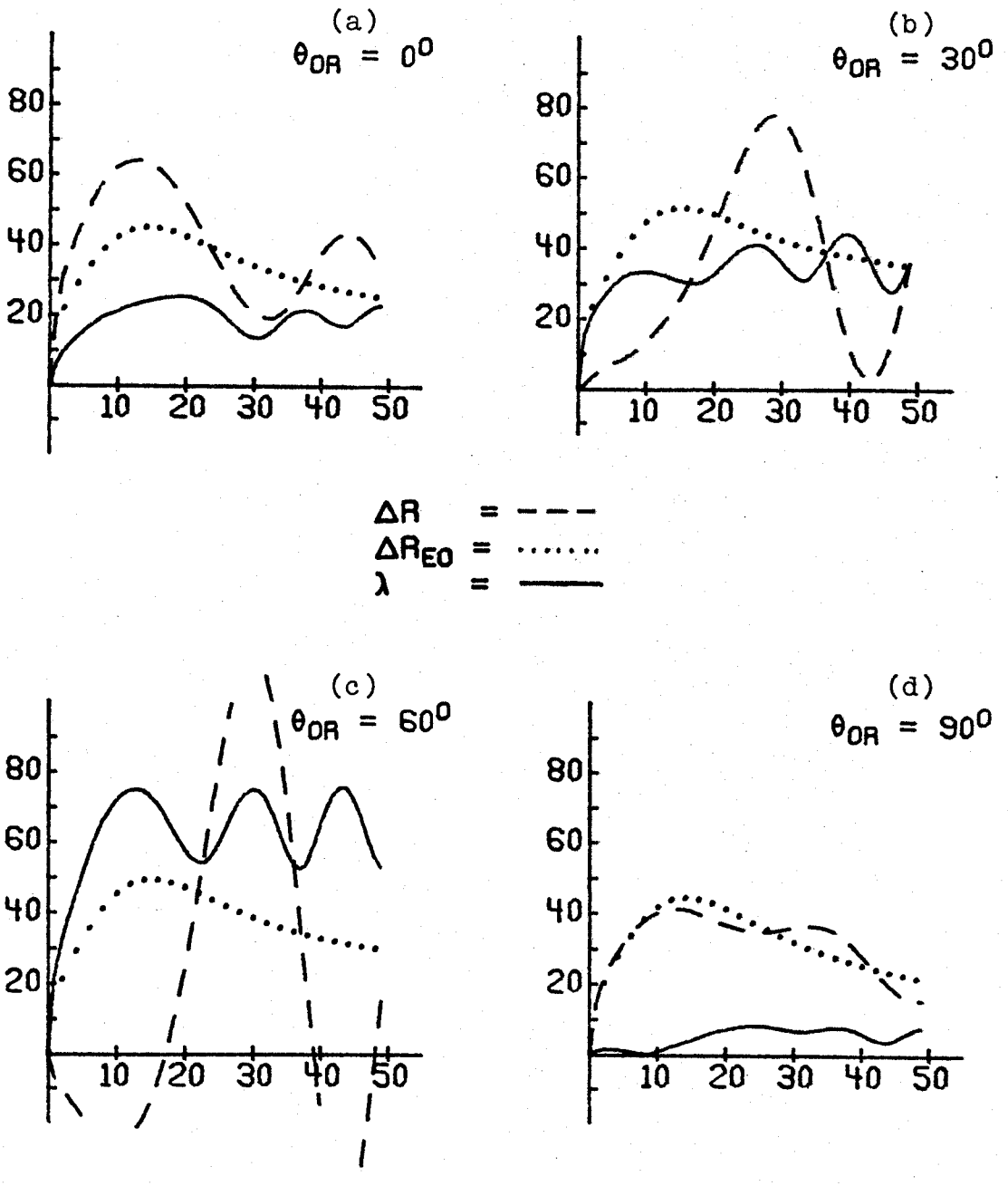

Figure 16. ΔR, ΔR_{EO} and λ vs. τ for N=3, E_f=30 MeV, τ_F=210, α=138° and h=1 plotted at $\theta=\theta_{or}$ for various θ_{or}'s. Ordinate values are in mils.

major to minor axis lengths, which ratio is plotted in Fig. 14.

Getting back to the interaction mentioned above, let us now examine the case of 90^{o} dees. With these the asymmetry in rf times of gap crossing causes Λ, after a few turns, to point at about 135^{o} from the positive p_x axis until precession becomes important. Comparison with θ_e at various θ_{or}'s shows that for $\theta_{or}=90^{o}$ the orbit asymmetry term driving $\Delta\Lambda$ is in phase with the rf driving term, while for $\theta_{or}=30^{o}$ the two are 180^{o} out of phase. This is why the pattern of large and small numbers shifts among the θ_{or} columns with decreasing α.

In summary, Table IV shows that $\theta_{or}=60$ gives the greatest λ's and, therefore, the best Q_x's for all dee angles except $\alpha=90^{o}$ where $\theta_{or}=90^{o}$ is superior, all other things being equal. Since the λ's are comparable with the ΔR_{EO}'s, it follows that the dee orientation must be given some thought whenever phase selection is desired and more important considerations do not dictate a specific θ_{or}.

3.2 Fielder Phase Curves

In this section we shall investigate the effects of varying the magnetic field contour with a fixed dee geometry, our study here concerning the effects of the different $\phi_F(\tau)$ we may produce. We use the initial phase, $\phi_o \equiv \phi_F(\tau=0)$ and the turn number τ_o such that $\phi_F(\tau=\tau_o)=0$, to characterize these curves. In any real situation, one would locate the ion source so that the CR corresponds to the centroid of the maximum intensity ion group from the source. Thus a change in ϕ_o corresponds to a change in the source-puller location relative to θ_1. Changing τ_o at a fixed ϕ_o is a change in the magnetic field.

The five curves used here are presented in Fig. 17. The curve parameters (ϕ_o,τ_o) are: A=(10°,20), B=(20°,10), C=(20°,20), D=(20°,30), E=(30°,20). Curves going strongly negative on early turns are not considered because of the possible associated axial defocusing difficulties. An attempt was made in all cases to obtain the straightest possible line from ϕ_o to zero for $0 \leq \tau \leq \tau_o$ with Fielder. Behavior of $\phi_F(\tau)$ on the first few turns is dominated by the central cone which extends some three or four inches in radius and causes the initial rapid fall-off in phase observed for $\tau<3$. Control over all other sections of $\phi_F(\tau)$ is about as good as is possible since the average trim coil spacing at M.S.U. is nearly half the magnet gap (6.75 in.).

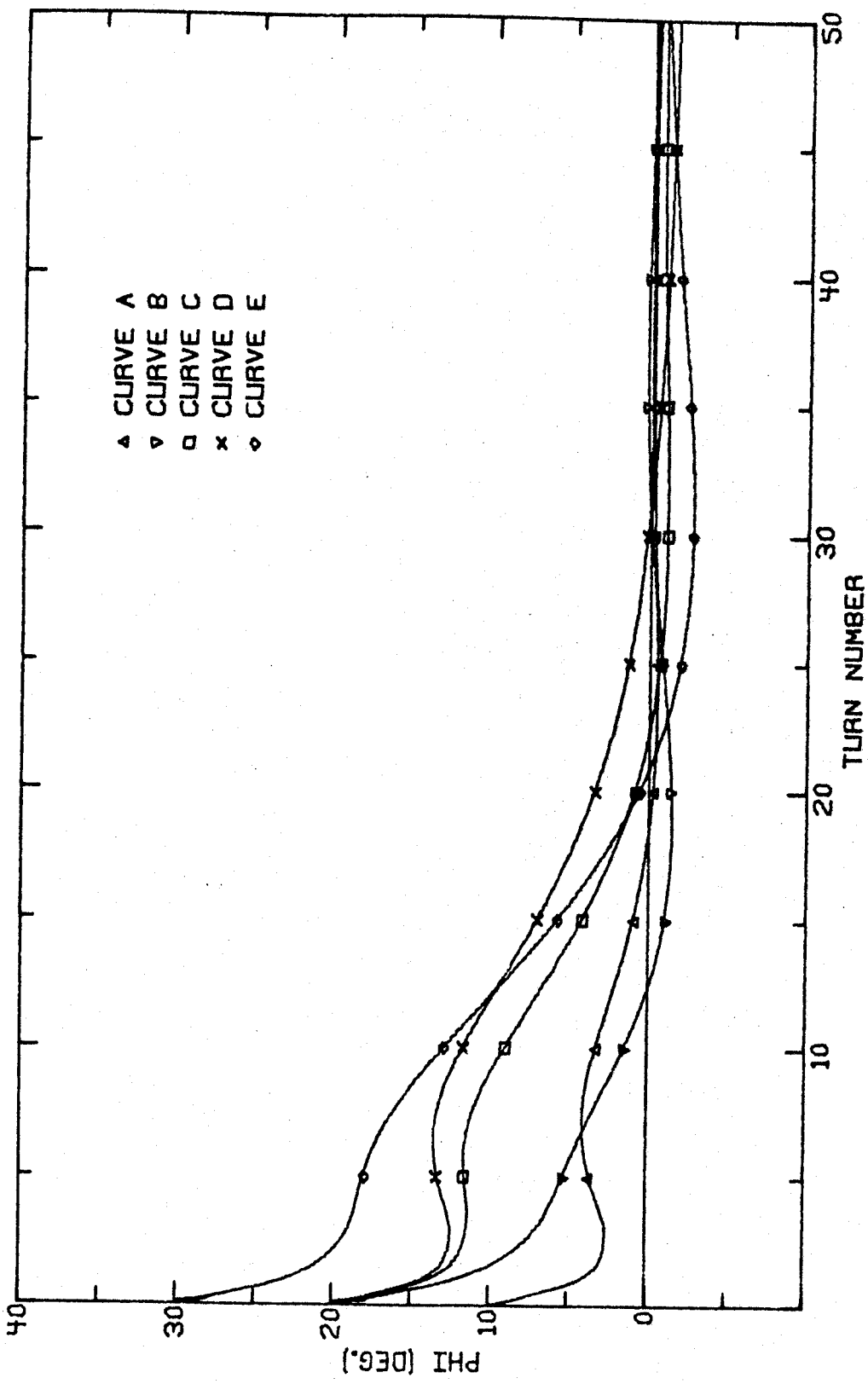

Figure 17. $\phi_F(\tau)$ for M.S.U. proton fields for h=1 and E_f=30 MeV. See text, p. 62, for curve parameters.

To obtain the data on ΔR_{EO} in Table V and on λ and λ_x in Table VI, we performed the procedure outlined in Sec. 2.2 for protons in three sector fields with E_f=30 MeV, α=138°, θ_{or}=0° and 60° and E_1=143 keV/turn. The columns labeled "Area" in Table V contain the results of using Eq. (8) and the different $\phi_F(\tau)$'s with trapezoidal rule integration. The values in parentheses in each column are "normalized" with the corresponding values for case E (note 1's in those columns). These normalized values of $\Delta R_{EO}(\theta_{or}=0°)$, $\Delta R_{EO}(\theta_{or}=60°)$ and "Area" should be the same for a given $\phi_F(\tau)$ if Eq. (8) is accurate. Agreement averages about 5% except for case A where 20% to 30% differences are average. Since all beams are similarly well centered, it should not be unexpected that the $\delta\phi_{CD}$'s are of similar magnitude in all cases. In case A, this means that on the very first turns ϕ_{CR} at θ_1 and θ_3 will be negative, decreasing ΔR_{EO} and accounting for the apparent discrepancies. Such evidence leads us to say that Eq. (8) is valid and useful.

The λ's of Table VI show that $\phi_F(\tau)$ for τ<10 or so is a most important characteristic and that the final λ is rather insensitive to the fine details of the $\phi_F(\tau)$ curves. Roughly one may group cases A with B, C and D, leaving E by itself, using the effect on λ as the distinguishing feature. From Fig. 17 it is seen that this grouping also is a rather natural one for the average of the $\phi_F(\tau)$'s,

TABLE V.--ΔR_{EO} at $\theta=\theta_{or}=0^{o}$ and $\theta=\theta_{or}=60^{o}$ for the $\phi_F(\tau)$ curves shown in Fig. 17. Included are the areas under the curves and values normalized to CASE E (parentheses).

N=3 h=1 $\alpha=138^{o}$ $E_1=143$ keV/turn $\Delta\phi=\pm2^{o}$

τ	θ_{or}	CASE A ΔR_{EO} (mils)	CASE A Area (rad-turn)	CASE B ΔR_{EO} (mils)	CASE B Area (rad-turn)	CASE C ΔR_{EO} (mils)	CASE C Area (rad-turn)	CASE D ΔR_{EO} (mils)	CASE D Area (rad-turn)	CASE E ΔR_{EO} (mils)	CASE E Area (rad-turn)
5	0.	6. (.113)	.46 (.204)	23. (.454)	1.04 (.462)	29. (.561)	1.40 (.622)	32. (.619)	1.49 (.662)	52. (1.)	2.25 (1.)
	60.	7. (.138)		24. (.490)		32. (.582)		32. (.645)		50. (1.)	
10	0.	11. (.162)	.79 (.221)	26. (.393)	1.30 (.363)	41. (.605)	2.31 (.645)	48. (.709)	2.62 (.732)	67. (1.)	3.58 (1.)
	60.	13. (.185)		29. (.411)		43. (.624)		51. (.730)		70. (1.)	
15	0.	12. (.171)	.95 (.219)	24. (.334)	1.28 (.295)	45. (.620)	2.85 (.657)	56. (.768)	3.40 (.783)	72. (1.)	4.34 (1.)
	60.	15. (.197)		27. (.352)		49. (.638)		61. (.789)		77. (1.)	
20	0.	11. (.162)	.96 (.211)	21. (.304)	1.15 (.253)	43. (.626)	3.02 (.664)	56. (.822)	3.81 (.837)	69. (1.)	4.55 (1.)
	60.	14. (.191)		24. (.322)		48. (.643)		62. (.843)		74. (1.)	

TABLE VI.--λ and λ_x at $\theta=\theta_{or}=0^{o}$ and $\theta=\theta_{or}=60^{o}$ for the same cases as shown in Table V.

		N=3 h=1 $\alpha=138^{o}$ $E_1=143$ keV/turn $\Delta\phi=\pm2^{o}$									
		CASE A		CASE B		CASE C		CASE D		CASE E	
τ	θ_{or}	λ (mils)	λ_x (mils)	λ (mils)	λ_x (mils)	λ (mils)	λ_x (mils)	λ (mils)	λ_x (mils)	λ (mils)	λ_x (mils)
5	0.	10.	-10.	12.	-12.	14.	-14.	16.	-16.	24.	-24.
	60.	45.	44.	42.	40.	45.	43.	51.	50.	59.	58.
10	0.	16.	-15.	16.	-15.	21.	-21.	21.	-20.	34.	-32.
	60.	62.	60.	60.	60.	69.	68.	72.	70.	87.	85.
15	0.	18.	-14.	18.	-15.	24.	-18.	24.	-17.	38.	-29.
	60.	60.	51.	66.	61.	74.	63.	71.	60.	93.	83.
20	0.	19.	-8.	20.	-10.	26.	-10.	24.	-8.	41.	-16.
	60.	47.	12.	56.	31.	61.	24.	56.	19.	80.	45.

particularly before turn 10. As $\phi_F(\tau)$ increases at a fixed τ from case A to case E, the asymmetry in the rf times of gap crossings between the two pairs of opposing gaps increases, thereby increasing $\Delta\lambda_{13}$ and decreasing $\Delta\lambda_{24}$ at $\theta_{or}=0$. This rf asymmetry driving term is not linear with phase since a factor of four change in $\phi_F(\tau)$ between cases A and E gives only a factor of two change in λ.

We present Table VII with ΔR_{EO} and λ vs. τ data for $\alpha=180^o$ and 90^o to demonstrate that we cannot treat α, θ_{or} and $\phi_F(\tau)$ disjunctive effects as being totally independent. One difficulty is brought out in the $\alpha=180^o$, $\theta_{or}=0^o$ data for case A showing larger λ's than for case C or even case E for $\tau>10$, apparently contradicting the last paragraph. But we mentioned above the negative phases occurring with curve A at θ_1 on early turns. On these turns, $\Delta\lambda=\delta\lambda_1+\delta\lambda_2$ instead of $\Delta\lambda=\delta\lambda_1-\delta\lambda_2$ as is true when all phases are positive as was assumed above. A second difficulty is the decrease in λ as one moves from case A to case E for $\alpha=90^o$ and $\theta_{or}=0^o$, again, an apparent contradiction. However, the explanation is that $\delta\lambda_1$ and $\delta\lambda_3$ are becoming closer in value. As $\phi_F(\tau)$ increases, $dV_{rf}(\theta_3)/dt-dV_{rf}(\theta_1)/dt$ increases since dV_{rf}/dt changes non-linearly with phase with the result that $\delta\lambda_3-\delta\lambda_1$ decreases because the energy denominators of Eq. (7) make $\delta\lambda_3<\delta\lambda_1$.

The last phase-curve-related changes in ΔR we wish to mention are the locations and magnitudes of the first maxima in both ΔR_{EO} and λ. For ΔR_{EO} there is only one

TABLE VII.--Comparison of ΔR_{EO} and λ for $\alpha=180^{o}$ and $\alpha=90^{o}$ at $\theta=\theta_{or}=0^{o}$ and $\theta=\theta_{or}=60^{o}$ to show a connection between α, θ_{or} and $\phi_{F}(\tau)$. See Fig. 17 for the corresponding $\phi_{F}(\tau)$ curves.

		N=3	h=1		E_1=143 keV/turn		$\Delta\phi=\pm2^{o}$	
			CASE A		CASE C		CASE E	
α	θ_{or}	τ	ΔR_{EO} (mils)	λ (mils)	ΔR_{EO} (mils)	λ (mils)	ΔR_{EO} (mils)	λ (mils)
180.	0.	5	8.	19.	28.	16.	50.	16.
		10	14.	29.	40.	27.	66.	30.
		15	16.	37.	43.	34.	70.	38.
		20	15.	41.	41.	38.	66.	43.
	60.	5	12.	31.	34.	37.	60.	52.
		10	18.	46.	47.	53.	73.	80.
		15	20.	47.	51.	53.	78.	87.
		20	18.	37.	49.	43.	74.	73.
90.	0.	5	1.	25.	23.	21.	48.	16.
		10	7.	38.	36.	34.	67.	25.
		15	9.	54.	40.	49.	73.	40.
		20	9.	61.	39.	58.	70.	50.
	60.	5	3.	35.	25.	39.	49.	44.
		10	11.	49.	42.	57.	74.	67.
		15	15.	50.	50.	60.	83.	74.
		20	15.	38.	49.	48.	81.	64.

maximum and its properties depend on how quickly $\phi_F(\tau)$ approaches zero. However, the $(E)^{-\frac{1}{2}}$ factor in Eq. (7) moves the maximum away from τ_o, the point of greatest ΔE. Table VIII shows τ for the maxima in ΔR_{EO} and λ and the respective maximum values. The strong correlation between τ_o and the location of maximum ΔR_{EO} is easily seen. In contrast, the location of the first maximum in the resonance driven λ's is independent of τ_o and depends on θ_{or} and θ_e.

This section may be summarized by saying that Q increases with increasing $\phi_F(\tau)$ at small τ, less than 15, perhaps. Q_{EO} unconditionally increases under this condition as does Q_x for $\theta_{or}=60^o$. However, the behavior of Q_x for $\theta_{or}=0^o$ is α dependent with a generally weaker tendency to increase than $Q_x(\theta_{or}=60^o)$. In any case, having ϕ_o as large as possible for a fixed τ_o will improve Q.

TABLE VIII.--Location and magnitude of the first maxima in ΔR_{EO} and λ at $\theta=\theta_{or}=0^{\circ}$ and $\theta=\theta_{or}=60^{\circ}$ for the $\phi_F(\tau)$ curves in Fig. 17.

N=3	h=1	$\alpha=138^{\circ}$	$E_1=143$ keV/turn		$\Delta\phi=\pm2^{\circ}$
CASE	θ_{or}	ΔR_{EO}		λ	
		Turn	Value (mils)	Turn	Value (mils)
A	0.	14	12.	19	19.
	60.	15	15.	13	63.
B	0.	9	26.	21	20.
	60.	10	29.	15	66.
C	0.	15	45.	19	26.
	60.	16	49.	13	75.
D	0.	19	57.	18	24.
	60.	19	62.	13	74.
E	0.	15	72.	20	41.
	60.	15	77.	14	93.

3.3 Energy Gain per Turn

We have now seen the effects of varying the dee and magnet geometries and the magnetic field contour for a fixed acceleration harmonic. The last geometry we have to vary is that of the orbits themselves, that is, the total turn number, τ_F, inside the magnetic field. For our purposes, $\tau_F=E_f/E_1$. A fixed τ_F implies equally good centering for any type of particle which may be used with a given h and, along with identical, or nearly so, $\phi_F(\tau)$ curves, ensures that all ΔR's, ΔR_{EO}'s and τ's will be the same in all such cases. Orbit calculations with $\tau_F=210$ for 15 and 36 MeV protons and 60 MeV helions show this very nicely for $\alpha=138^o$ and h=1.

One may, of course, design different τ_F's into one's machine, usually with a tendency toward lower numbers to enhance turn separation and extraction, although this leaning is limited by voltage holding capabilities and the α chosen. Unlike M.S.U., most cyclotrons operate near their maximum dee voltage so that τ_F changes with particle type and E_f. In either case, as demonstrated in the previous section, both ΔR_{EO} and λ will depend on the $\phi_F(\tau)$ involved, which, therefore, must be specified before we continue. In making a comparison between cases of different τ_F's, we consider two viable alternatives. First, we may take $\phi_F(E)$ as invariant (or as nearly so as Fielder will allow), in which case we already know enough to state that, at least

after it reaches its maximum, ΔR_{EO} should vary roughly as $(E_1)^{-\frac{1}{2}}$ at a fixed τ by Eqs. (7) and (8). Notice also that, while decreasing E_1 should decrease the resonant driving "force" acting to increase λ, it will also maintain ϕ_{CR} at a higher value over more turns, increasing the resonant drive. Therefore, Q is not a sensitive function of E_1 and increasing E_1 cannot be expected to improve Q greatly.

The second alternative is to maintain $\phi_F(\tau)$ as constant. Doing so introduces a rather subtle effect so we therefore present Table IX comparing data on $\phi_F(\tau)$, x, p_x (for the CR) ΔR_{EO} and λ for protons with E_f=30 MeV and E_1 values such that τ_F=120, 210, and 300. Since the $\phi_F(\tau)$ curves are the same (at least near the machine center), the integral in Eq. (8) is constant and ΔR_{EO} should vary as $(E_1)^{\frac{1}{2}}$, which can be verified as true from the table entries. Values of λ should likewise change by this factor since all resonance driving terms are combinations of terms similar to the left hand side of Eq. (7). However, ΔE depends on the $\delta\phi_{CD}$'s of Eq. (3). The x-p_x data included in Table IX shows that centering improves with increasing τ_F, as should seem intuitively correct, but more slowly than as $(E_1)^{\frac{1}{2}}$. Then $\delta\phi_{CD}$, at a given gap and τ, actually tends to decrease with decreasing τ_F since the denominator of Eq. (3) increases faster than the numerator. This decreases the rf asymmetry driving term, at a rate other than proportional to $(E_1)^{\frac{1}{2}}$. It is this difference in rates, between the

TABLE IX.--Comparison of orbit properties in an M.S.U. proton field for various values of E_1 at fixed E_f=30 MeV and $\theta=\theta_{or}=0^{\circ}$.

N=3 h=1 $\alpha=138^{\circ}$ $\Delta\phi=\pm2^{\circ}$

τ	τ_F	ϕ_{CR} (deg)	x (mils)	p_x (mils)	ΔR_{EO} (mils)	λ (mils)
5	300	6.02	26.	214.	18.	9.
	210	7.74	33.	262.	24.	11.
	120	7.28	59.	292.	33.	8.
10	300	5.71	7.	179.	21.	13.
	210	4.52	23.	206.	28.	16.
	120	2.93	11.	216.	36.	10.
15	300	3.18	16.	150.	23.	16.
	210	1.27	16.	164.	28.	19.
	120	1.57	-16.	183.	34.	12.
20	300	.56	9.	125.	22.	17.
	210	-.07	8.	134.	25.	21.
	120	.40	-15.	171.	31.	12.

variations with E_1 in the l.h.s. of Eq. (7) at a constant $\phi_F(\tau)$ and in $\delta\phi_{CD}$ that gives rise to the larger λ values for τ_F=210 compared with either of the other cases.

Inspection of the data also shows that the 210 turn geometry is possibly close to producing the largest possible λ's under the condition of fixed $\phi_F(\tau)$. Since Q is insensitive to τ_F (the table shows only a 20% variation with a factor of 2.5 change in τ_F), no computer time was spent attempting to find this optimal τ_F. It is interesting to note, however, that in this case, as for constant $\phi_F(E)$, Q does not increase monotonically with E_1 as might be expected at first glance.

3.4 Acceleration Harmonic Number

The final acceleration parameter to be investigated for a three sector field is the acceleration harmonic h. Three effects should arise with increasing h. First is simply the fact that for a fixed α the rf times for zero phase gap crossings will change so that the rf term driving disjunction will be different for each h value. Second is the increased importance of the orbit form factor phase shifts by the factor h. Third is the multiplication by h in Eq. (3) for $\delta\phi_{CD}$.

The data presented in Table X for h=2 is for a 15 MeV deuteron field with the same τ_F(=210) as in Sec. 3.1 and 3.2. We treat only 138° and 90° dees for h=2, but the particle type and final energy are quite arbitrary: 7.5 MeV protons and 30 MeV alphas give equivalent results. The $\phi_F(\tau)$ curve may be found in Fig. 18.

Most easily explained in detail is the α=90° case since zero phase gap crossings occur at the rf wave peaks. ΔR_{EO}'s should be somewhat below those listed in Table III for h=1 since this $\phi_F(\tau)$ is about 20% below curve C of Fig. 17. Values of λ are between 4 and 10 mils for all values of θ_{or} and τ, since rf asymmetry is almost non-existant. The excellent centering which we have previously associated with α=90° leads to very small $\delta\phi_{CD}$'s which might affect the rf asymmetry, even with the extra factor of two.

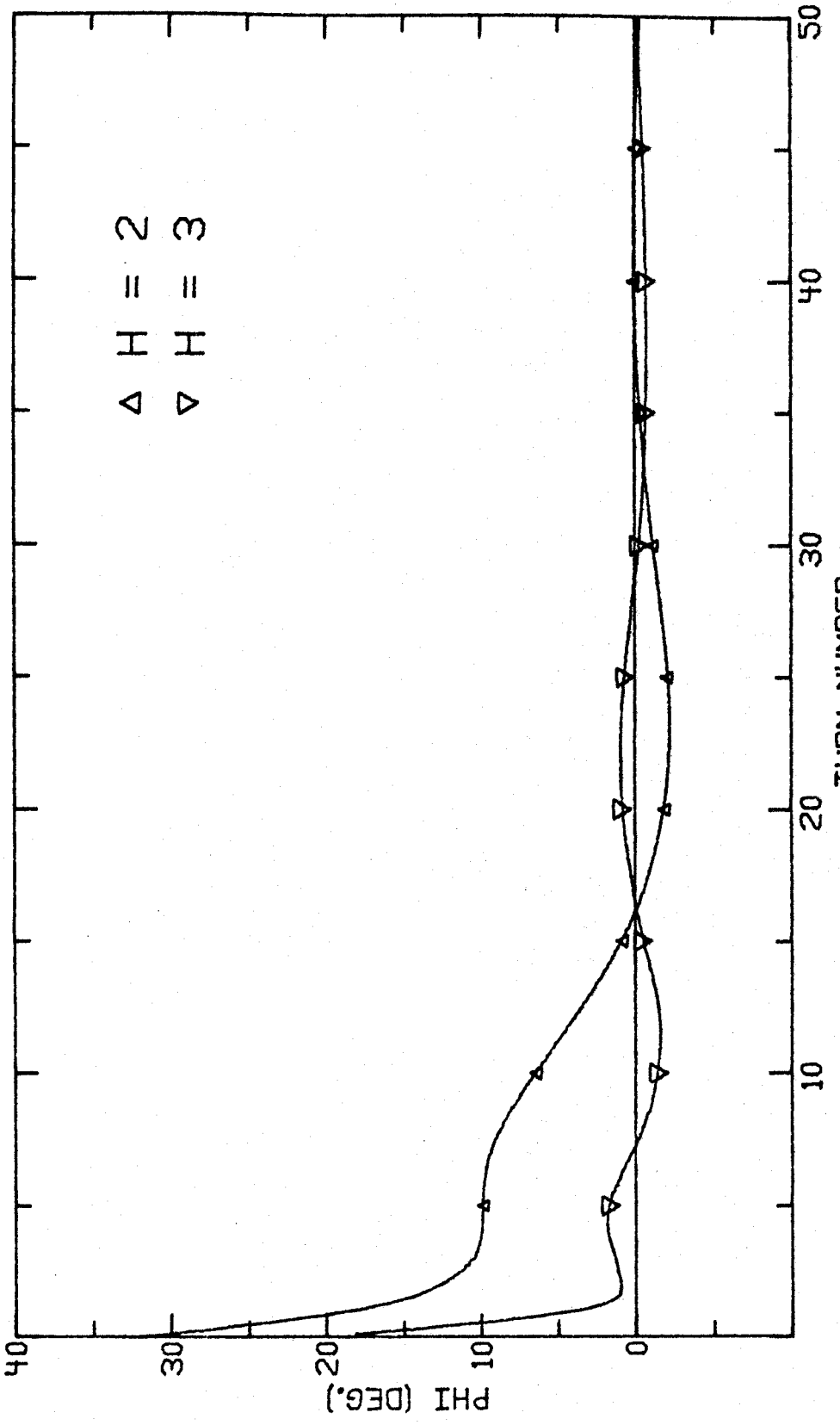

Figure 18. $\phi_F(\tau)$ for an M.S.U. deuteron field for h=2 and E_f=15 MeV and an M.S.U. C^{3+} field for h=3 and E_f=27 MeV.

TABLE X.--ΔR_{EO}, λ and λ_x at $\theta=\theta_{or}$ for various dee angles on h=2. The magnetic field used corresponds to the $\phi_F(\tau)$ shown in Fig. 18.

		N=3	h=2	E_1=68 keV/turn	$\Delta\phi=\pm2^\circ$		
			$\alpha=138^\circ$			$\alpha=90^\circ$	
τ	θ_{or}	ΔR_{EO} (mils)	λ (mils)	λ_x (mils)	ΔR_{EO} (mils)	λ (mils)	λ_x (mils)
5	0.	26.	12.	-4.	26.	6.	-1.
	30.	31.	19.	11.	33.	7.	11.
	60.	29.	10.	1.	30.	6.	-3.
	90.	21.	21.	-2.	24.	5.	-15.
10	0.	35.	23.	-1.	32.	5.	1.
	30.	44.	28.	21.	43.	8.	2.
	60.	41.	16.	-2.	40.	7.	0.
	90.	29.	28.	-28.	30.	5.	-1.
15	0.	37.	33.	8.	31.	4.	2.
	30.	48.	34.	31.	44.	9.	6.
	60.	45.	20.	-11.	40.	8.	5.
	90.	30.	40.	-39.	30.	5.	0.
20	0.	33.	38.	21.	25.	3.	3.
	30.	45.	35.	34.	40.	10.	9.
	60.	41.	24.	-21.	35.	10.	10.
	90.	25.	51.	-37.	21.	4.	2.

The $\delta\lambda$'s at opposing gaps are almost equal, differing mainly only by the energy denominator of Eq. (7), and, therefore, nearly cancel. As a measure of the orbit symmetry involved, Fig. 19 gives p_x asymmetry values for AEO's with $\alpha=138^\circ$ vs. percentage of E_f on h=1, 2 and 3. By Sec. 2.3 we expect values for $\alpha=90^\circ$ to be lower than the h=2 curve actually plotted, which is already lower than the h=1 case presented for comparison.

Of greater interest is a comparison of ΔR_{EO} and λ data for 138° dees and h=2 in Table X and previously given data for h=1 (Tables III, V and VI). The h=2 ΔR_{EO} data shows larger variations (approximately twice as large) with θ_{or} as follows from the more important form factor phase shifts. As to the data on λ, note first that h=2 does not demonstrate variations with θ_{or} as large as does h=1, nor does it have the very strong preference (in terms of larger Q_x) for $\theta_{or}=60^\circ$ and the poor showing at $\theta_{or}=90^\circ$ discussed before for h=1. In fact, $\theta_{or}=90^\circ$ gives the best Q_x on h=2.

To understand these results one must realize that the zero phase gap crossings occur as in Fig. 20. (Cf. Fig. 9.) Large phases now tend to produce small $\delta\lambda$'s at θ_1 and large $\delta\lambda$'s at θ_2, in direct contrast to the h=1 situation. Small phases are now to be preferred at θ_1 for larger resonant increase in λ. The better Q_x for $\theta_{or}=90^\circ$ may now be seen to be connected with the very low phase occurring at gap 1 and the very large phase at gap 3. The reversal in relationship between θ_{or} and λ is the reversal in the sign of

Figure 19.--Orbit asymmetries for $\alpha=138^{o}$ in the N=3 fields for h=1, 2, 3 used in Secs. 3.1 and 3.4. The p_x asymmetry is defined in Sec. 2.3. The curve plotted with squares is for $\tau_F=120$. All others have $\tau_F=210$. The h=1 curve is the same as in Fig. 3.

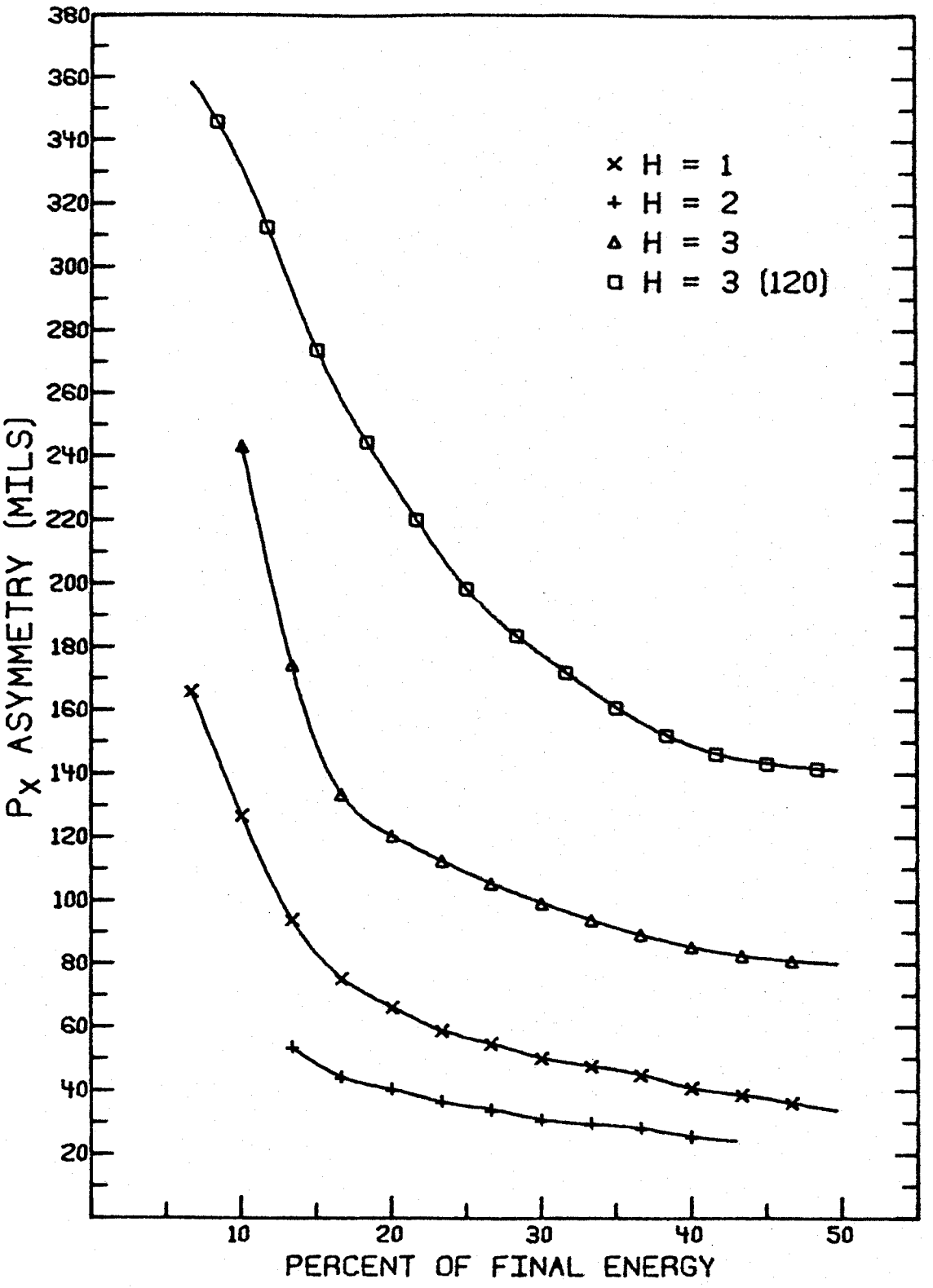
× H = 1
+ H = 2
△ H = 3
□ H = 3 (120)
P_X ASYMMETRY (MILS)
380
360
340
320
300
280
260
240
220
200
180
160
140
120
100
80
60
40
20
10
20
30
40
50
PERCENT OF FINAL ENERGY

Figure 19.

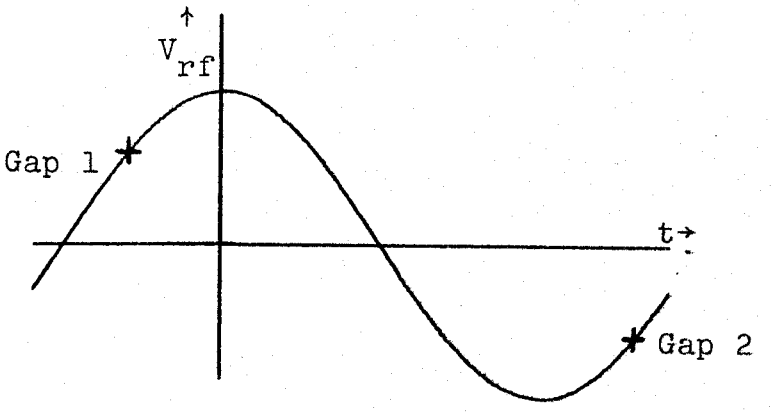

Figure 20. Zero phase gap crossing times with $\alpha=138^{o}$ and h=2. Compare with cross locations in Fig. 9.

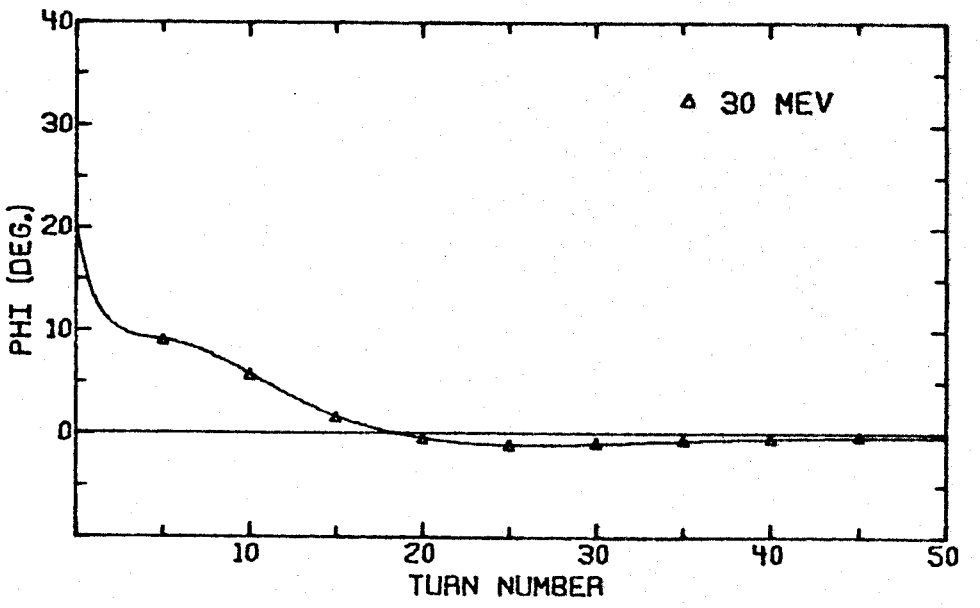

Figure 21. $\phi_F(\tau)$ for an N=4, 30 MeV proton field.

dV_{rf}/dt at each gap when comparing h=1 and h=2.

Again referring to Fig. 19, we see that AEO asymmetry greatly increases with third harmonic operation. This, along with the fact that $\delta\phi_{CD}$ now includes a factor of three, makes acceleration very difficult in some cases and impossible in others: one finds that one cannot decelerate particles backward past 1 or 2 MeV to find source positions using $\alpha=138^{o}$ and $\tau_F=210$. As demonstrated by Learn, et al.,[15] we may expect 90^{o} dees to perform adequately if we switch to a 120 turn geometry although 138^{o} dee performance is still unsatisfactory as supported by the large asymmetries in Fig. 19. (We should mention that our difficulties on h=3 stem from our centering requirement for the CR.) We shall, therefore, consider only $\alpha=180^{o}$ and 90^{o} for h=3 and will, for convenience, use the same field as Learn. For further details on this problem and the performance of 60^{o} dees, we refer the reader to Learn, et al.

The relevant data is contained in Table XI for 27 MeV C^{+3} ions. Again we see the dependence of ΔR_{EO} on θ_{or} becoming stronger from the form factor effect for both $\alpha=180^{o}$ and 90^{o}. The extremely large λ values observed (as much as an order of magnitude greater than most of our previous cases) are due partially to the increased sensitivity to the gap-crossing resonance shown in Fig. 19 and partially to values of $\delta\phi_{CD}$ of 20^{o} to 30^{o} between gaps on early turns. This is also, of course, the reason for the order of magnitude change in λ between $\theta_{or}=30^{o}$ and 90^{o}.

TABLE XI.--ΔR_{EO}, λ and λ_x at $\theta=\theta_{or}$ for various dee angles on h=3. The magnetic field used corresponds to the $\phi_F(\tau)$ shown in Fig. 18.

		N=3	h=3	E_1=227 keV/turn	$\Delta\phi=\pm2^\circ$		
			$\alpha=138^\circ$			$\alpha=90^\circ$	
τ	θ_{or}	ΔR_{EO} (mils)	λ (mils)	λ_x (mils)	ΔR_{EO} (mils)	λ (mils)	λ_x (mils)
5	0.	4.	77.	-85.	-2.	88.	3.
	30.	22.	73.	76.	6.	198.	-40.
	60.	14.	102.	100.	-14.	57.	8.
	90.	-6.	60.	-55.	-26.	4.	-1.
10	0.	8.	116.	-104.	-3.	130.	-32.
	30.	23.	78.	78.	30.	400.	-189.
	60.	12.	143.	139.	-22.	94.	51.
	90.	-17.	82.	-71.	-54.	36.	-7.
15	0.	9.	148.	-67.	-13.	119.	-77.
	30.	22.	70.	36.	46.	532.	-379.
	60.	11.	143.	82.	-13.	123.	113.
	90.	-14.	80.	-38.	30.	29.	0.
20	0.	12.	146.	29.	-16.	89.	84.
	30.	23.	89.	-40.	12.	109.	-60.
	60.	12.	109.	-69.	28.	129.	120.
	90.	-17.	52.	29.	28.	30.	17.

In summary we can say that Q is highly dependent on h because of the different gap crossing times involved at fixed α. A phase selection system which works well on one harmonic should not be expected to perform satisfactorily on other harmonics. For example, with 90^{o} dees, citing the best values at any turn in each case one finds $Q(h=1)/Q(h=2) \simeq 4$ at $\theta_{or}=0^{o}$.

3.5 Four Sector Fields

Lastly we wish to consider ΔR in a four sector field. We shall again consider a 30 MeV proton field. The $\phi_F(\tau)$ for this field is in Fig. 21 while the ν_r and ψ curves are in Fig. 22 and eigen-ellipse properties are in Fig. 23. Both ψ and ν_r as functions of energy are smaller in four than in three sector fields, as are the eigen-ellipse eccentricities.

Unaffected by the change in N are Eqs. (7) and (8), as supported by comparing the ΔR_{EO} columns in Tables XII and V. The same form factor variations with θ_{or} are present in ΔR_{EO} and the magnitudes are consistent since the area under $\phi_F(\tau)$ of Fig. 21 is 70% that under curve C in Fig. 17.

What we must give some attention to is Q_x. Of great importance to Q_x is the fact that the field symmetry now eliminates the gap-crossing resonance so that AEO's are quite symmetric at all energies and dee angles (cf. Fig. 2 and6). Accordingly, the particle orbits are symmetric, with CR $x\text{-}p_x$ histories all appearing in one quadrant ($x<o, p_x>o$). This is quite a contrast to the N=3 case of Fig. 3 and 4.

Before looking at any data we may conclude from our previous work that $\Delta\lambda$ will be significantly smaller than for N=3 because of smaller $\delta\phi_{CD}$'s accompanying the more symmetric orbits producing more equal disjunctions at opposite gaps. The oscillatory structure of λ vs. τ will

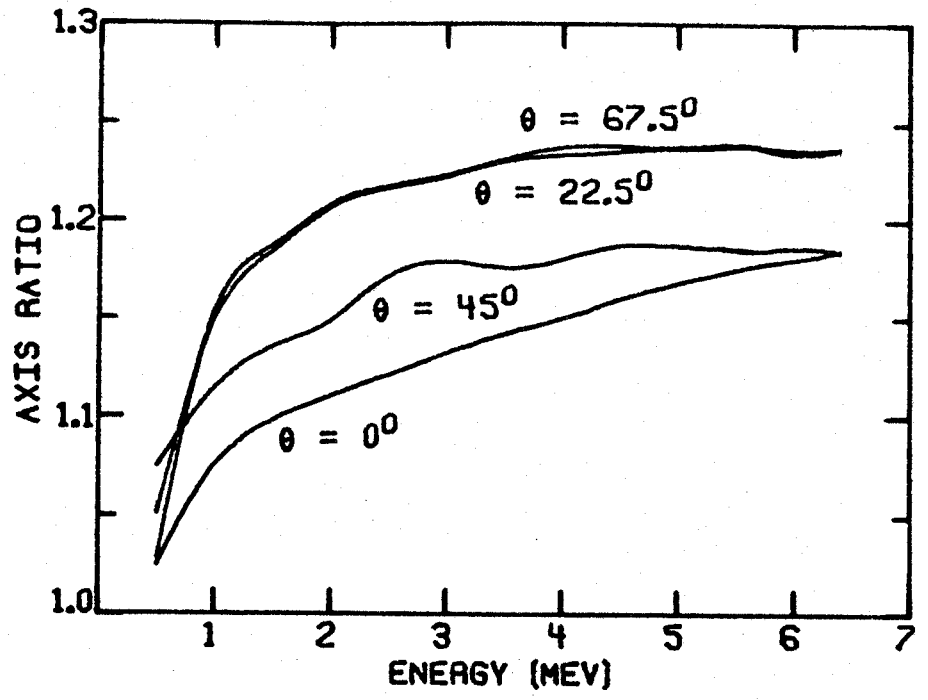

Figure 22. Eigen-ellipse axis length ratios vs. energy for a proton field with N=4, E_f=30 MeV. Note change of ordinate scales from Fig. 14.

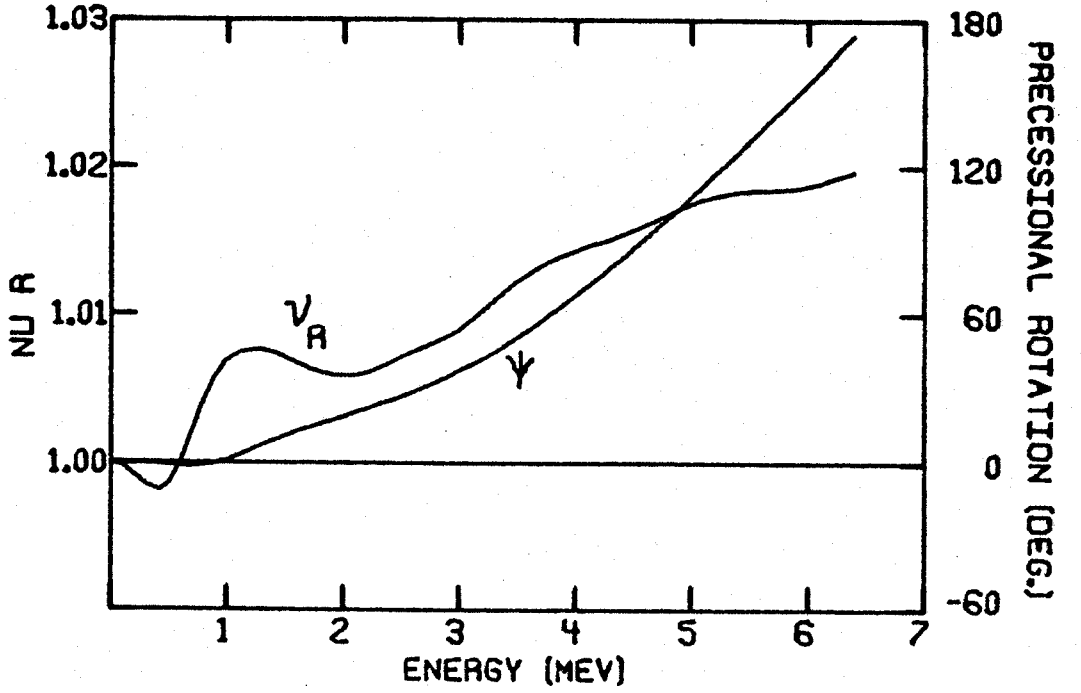

Figure 23. ν_r and ψ(see Eq. 11) vs. energy in the field used for Fig. 22. Note change of ordinate scales from Fig. 15.

also be decreased since the precession is slower and the relative orientation of Λ and eigen-ellipse at a given azimuth is of lesser import. From the resonance viewpoint, although the resonant condition will exist over a significantly larger number of turns than in the three sector field due to slower change in ν_r, only the rf driving term will be large with a negligible field asymmetry driving term. The conclusion to be reached then is that a four sector cyclotron as at Maryland will have a small Q_x value and one which is insensitive to θ_{or} when compared with a similar N=3 machine.

We present ΔR_{EO} and λ compiled in Table XII and Fig. 24 (analogous to Table III and IV and Fig. 16) to bear out these assertions. Dependence on θ_{or} is qualitatively the same as for N=3 for both ΔR_{EO} and λ, with the extra feature of decreasing λ with increasing τ for $\theta_{or}=0^{\circ}$, 22.5° and $\alpha=180^{\circ}$. This is mainly an energy effect depending on $(E)^{-\frac{1}{2}}$ in Eq. (7) which we can now see because it is not masked by any field asymmetry. The quantitative dependence of λ on θ_{or} is much weaker at each α value (for $\alpha=90^{\circ}$ compare the worst case λ change of 20% here to the N=3 worst case change of 400%). Since only the rf driving term is appreciable it is hardly surprising that we find a very strong α dependence. Finally, notice that there exists the same preference as with N=3 in terms of larger Q_x's for θ_{or} to be a hill center.

In summary, for h=1 we see that a four sector field offers one much less sharply defined choices toward

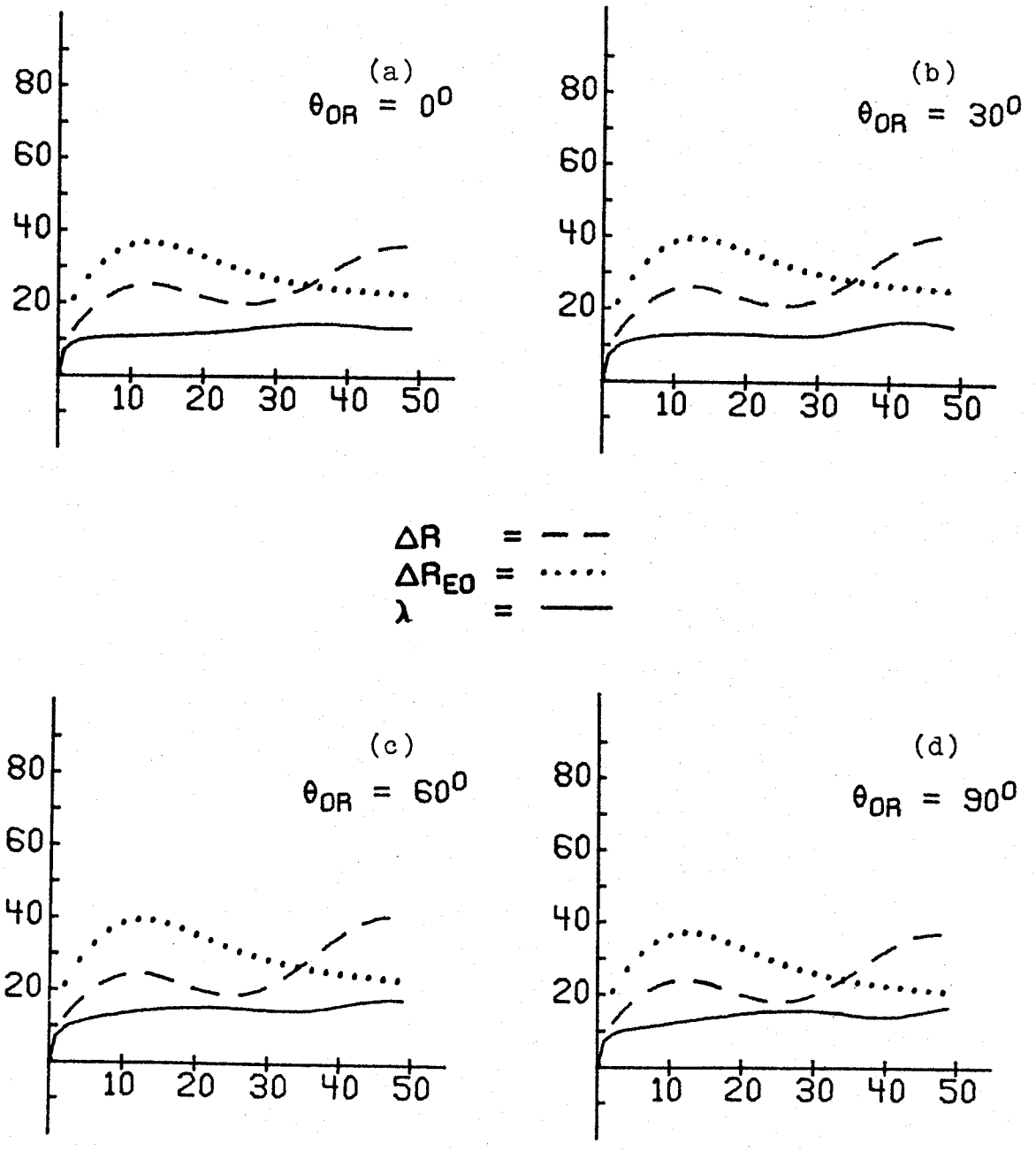

Figure 24. ΔR_{EO}, λ and ΔR vs. τ plotted at $\theta=\theta_{or}$ for various θ_{or}'s for N=4, E_f=30 MeV, $\alpha=138^o$, τ_F=210 and h=1. Ordinate values are in mils.

TABLE XII.--ΔR_{EO}, λ and λ_x at $\theta=\theta_{or}$ for various dee angles and N=4. The magnetic field used corresponds to the $\phi_F(\tau)$ shown in Fig. 21.

N=4 h=1 E_1=143 keV/turn $\Delta\phi=\pm2^\circ$

τ	θ_{or}	$\alpha=180^\circ$			$\alpha=138^\circ$			$\alpha=90^\circ$		
		ΔR_{EO} (mils)	λ (mils)	λ_x (mils)	ΔR_{EO} (mils)	λ (mils)	λ_x (mils)	ΔR_{EO} (mils)	λ (mils)	λ_x (mils)
5	0.	28.	6.	6.	27.	10.	9.	21.	27.	26.
	22.5	28.	7.	7.	28.	12.	11.	23.	29.	29.
	45.	29.	9.	9.	28.	12.	11.	22.	30.	29.
	67.5	29.	8.	8.	27.	11.	10.	20.	28.	28.
10	0.	36.	4.	4.	35.	11.	11.	30.	35.	35.
	22.5	36.	7.	7.	37.	13.	12.	34.	37.	37.
	45.	38.	9.	9.	37.	15.	14.	33.	40.	40.
	67.5	37.	8.	7.	35.	12.	12.	35.	37.	36.
15	0.	36.	4.	4.	36.	11.	11.	32.	40.	39.
	22.5	37.	6.	6.	39.	13.	13.	37.	41.	40.
	45.	38.	9.	9.	39.	13.	13.	36.	46.	46.
	67.5	37.	8.	7.	37.	14.	13.	30.	46.	44.
20	0.	33.	4.	3.	33.	12.	11.	29.	44.	39.
	22.5	34.	6.	5.	36.	13.	13.	35.	43.	41.
	45.	35.	9.	8.	36.	16.	14.	33.	50.	48.
	67.5	34.	8.	6.	33.	15.	12.	27.	52.	45.

optimizing Q. Only for 90^{o} dees is there a strong dependence of ΔR on anything other than energy difference and this is independent of θ_{or}. Even after correcting for the difference in $\phi_F(\tau)$ curves, the best possible Q for N=4 will be seen to be worse than the best for N=3.

These same general statements should also apply to higher harmonic operation. One further effect we would find is lessening of the variations in ΔR_{EO} with θ_{or} because the form factor $F(\theta)$ varies as N^{-2}.

4. CONSEQUENCES FOR PHASE SELECTION

4.1 Locating Phase Selective Slits

To this point we have presented data which can certainly be used as at least a semi-quantitative guide showing how ΔR varies with various accelerator parameters. The question to discuss now is how to use this information in planning for a phase selection system in either an existing or a proposed machine. We shall assume that a CR as defined in Sec. 2.1 exists in either case and that the aim is to locate a slit or slits, centered on this ray, for their most effective use at the lowest possible energy. That is to say, we wish to know where Q of Eq. (10) is maximum in a region where thermal and radiation problems will be least severe and where turns in the unfiltered beam are still separated.

In general, slits could be placed anywhere along the CR and perform phase selection. With few exceptions, phase displaced particles will always have some radial separation due to their energy difference, and, as a first order approximation, one would, if one could, place a slit where ΔR_{EO} was maximum. This approximation amounts to simply neglecting λ and is a good approximation for cases like $\alpha=180^{o}$, N=4, h=1 or $\alpha=90^{o}$, N=3, h=2. One can combine Eqs. (7), (8), and (6) to write

$$Q_{EO} = \Delta R_{EO}/\Delta\phi = -(R_o/2)\langle\phi_F\rangle_\tau(1 + F(\theta)) \qquad (12)$$

an expression which the data in Sec. 3.2 showed to be fairly accurate. To apply Eq. (12) to all azimuths, one must require that δR_{EO} from Eq. (7) at any gap is much less than ΔR_{EO} used above. We shall assume that τ is large enough for such to be the case so that Q_{EO} is independent of θ in all our discussion in this section.

In the other cases, e.g., $\alpha=90^o$, $\theta_{or}=90^o$, N=3, h=1 or $\alpha=90^o$, $\theta_{or}=30^o$, N=3, h=3, where λ and ΔR_{EO} are of comparable magnitude, they must be added, with due consideration given to the orientation of Λ, to determine the optimal slit location. In the examples previously given in Figs. 16 and 24, we have included the end results of these considerations: ΔR vs. τ. Tabulated results in the form of Q values fill Tables XIII, XIV and XV. Maxima in these curves obviously are optimal slit locations, but the curves are accurate only near the azimuths at which they are drawn. Since we are formally presenting data only at $\theta=\theta_{or}$ (Sec. 5.3 contains data at other angles), we must discuss the principles governing these curves so we may have a basis for deciding what ΔR will be at arbitrary angles.

At this point we return to the data on λ_x which has been supplied in most of the tables of Chapter 3 but has not been formally discussed. These λ_x depend not only on λ, which we have talked about at length, but also on the orientation of Λ in x-p_x space. For $\alpha=180^o$, before the

TABLE XIII.--Turn number and value of the best Q at $\theta=\theta_{or}$ and $\theta=\theta_{or}+\pi$ for various dee angles on h=1. This table complements Tables III and IV.

	N=3 h=1 E_1=143 keV/turn					
	$\alpha=180^\circ$		$\alpha=138^\circ$		$\alpha=90^\circ$	
θ_{or}	τ	Q (mils/deg)	τ	Q (mils/deg)	τ	Q (mils/deg)
0.	12	16.5	13	16.1	28	20.8
180.	29	18.4	29	15.5	9	20.8
30.	28	17.3	29	19.6	26	19.2
210.	11	19.6	12	22.4	10	20.2
60.	29	23.8	30	28.3	30	21.6
240.	11	21.1	11	25.2	11	24.5
90.	12	13.8	12	10.4	31	24.0
270.	26	10.6	14	15.0	11	24.6

TABLE XIV.--Turn number and value of the best Q at $\theta=\theta_{or}$ and $\theta=\theta_{or}+\pi$ for various dee angles on h=2 and h=3. This table complements Tables X and XI.

θ_{or}	N=3 h=2 E_1=68 keV/turn $\alpha=138^{o}$ τ	Q (mils/deg)	$\alpha=90^{o}$ τ	Q (mils/deg)	N=3 h=3 E_1=227 keV/turn $\alpha=180^{o}$ τ	Q (mils/deg)	$\alpha=90^{o}$ τ	Q (mils/deg)
0.	9	9.1	10	7.9	9	28.0	18	18.6
180.	25	17.1	12	7.9	9	-32.0	17	-38.4
30.	8	3.6	10	10.4	8	-14.0	18	110.6
210.	18	18.6	15	12.5	8	27.0	19	-89.8
60.	10	15.6	22	10.1	9	-31.5	18	-33.7
240.	10	6.5	13	9.6	8	28.6	18	-33.7
90.	15	17.1	9	7.7	7	16.0	26	-13.0
270.	34	12.8	11	7.4	8	-19.5	9	-10.0

TABLE XV.--Turn number and value of the best Q at $\theta=\theta_{or}$ and $\theta=\theta_{or}+\pi$ for various dee angles with N=4. This table complements Table XII.

	N=4 h=1 E_1=143 keV/turn					
	$\alpha=180^\circ$		$\alpha=138^\circ$		$\alpha=90^\circ$	
θ_{or}	τ	Q (mils/deg)	τ	Q (mils/deg)	τ	Q (mils/deg)
0.	12	8.0	12	6.3	21	-2.7
180.	11	10.3	12	12.8	13	19.2
22.5	12	8.0	12	6.6	21	-1.5
202.5	11	10.9	12	13.9	14	21.3
45.	12	7.4	11	6.2	21	-3.9
225.5	11	11.9	12	14.4	14	22.3
67.5	12	10.1	11	6.0	21	-4.6
247.5	11	11.5	12	13.3	13	20.1

precession angle ψ becomes large, Λ parallels the x axis. However, for any other α, the interactions represented by the vectors K_1 and K_2 in Eq. (9) cause Λ to take on some other orientation. The sign of λ_x results from the dependence of ϕ_{CR} on gap number. For example, in Fig. 16 ΔR may be seen to start as the sum of the other two curves for $\theta=0^o$ and 90^o ($\lambda_x \leq 0$) and their difference for $\theta_{or}=30^o$ and 60^o ($\lambda_x \geq 0$).

If we define μ as the angle between Λ and the x axis so that we could calculate it as $\mu=\text{Tan}^{-1}(\lambda_p/\lambda_x)$, we find that $\mu \approx \mu_o$, a constant, over the early turns until precession takes over. Given such a μ_o at $\theta=0$, for instance, on a turn where ψ is small, one may rewrite Eq. (4) as

$$\Delta R(\theta,\tau) = \Delta R_{EO}(\tau) + \lambda(\tau)\cos(\nu_r\theta-\mu_o+\psi(\tau)). \qquad (13)$$

This equation is particularly useful for τ large enough (usually $\tau>10$) that ΔR_{EO} is independent of θ and λ varies only according to eigen-ellipse effects. With Eq. (13) and the data in Chapter 3, one can now determine ΔR at any location in his machine. (Strictly speaking, given only the data in Chapter 3, one must resolve the sign ambiguity involved with $\mu_o=\text{Cos}^{-1}(\lambda_x/\lambda)$ by obtaining the difference between μ_o and μ on some later turn and comparing that difference to the $\Delta\psi$ expected for the corresponding $\Delta\tau$.)

Suppose we have now positioned one slit so that Eq. (13) predicts a satisfactory Q. To determine the necessity for, and possible placement of, any second slit, we refer to Sec. 2.5 to remind ourselves that particles displaced in p_x from the CR will display significant phase displacements from the CR during their acceleration history. We must then consider eliminating these particles. Since the incoherent oscillation amplitude of such particles is usually greater than their ΔR_{EO} from the CR, the proper location of a slit follows from considering precessional motion.

There is one important difference between the spatial and temporal displacement cases which makes a two slit phase selection system necessary. At θ_{or} and before ψ becomes important, μ_o is usually small while a vector similar to Λ on the x-p_x plane between rays of $\pm\delta p_x$ is 90^o "out of phase" with Λ, approximately parallel to the p_x axis. This means that to achieve total phase selection requires two slits either 90^o apart on the same turn or ¼ precession cycle apart on the same azimuth. Having both slits the same size yields a final beam which occupies a compact area in phase space: its area and all dimensions are small. Such a beam will retain its high quality (small phase width and x-p_x area) through the extraction region and present a small energy width and emittance to the beam transport system.

One assumption implicit in the discussion of this section is that we are dealing with separated turns. In fact, such would not be the case for τ=20-30, where we would place our slits, because of the large beam phase width to that point. To cure this problem, the M.S.U. cyclotron contains a slit (10 mils wide for h=1 proton operation) about 180^{o} away from the source-puller. This "half turn" slit performs a rough phase selection, passing at most two particle groups at different centroid phases, each with a relatively narrow phase width. One group is the maximum intensity group, the centroid of which corresponds to our CR. It is this group which the cyclotron is tuned to accelerate and on which our slits perform the final phase selection. The other group is lost on the jaws of the first slit, the difference in centroid phases not being enough to cause overlapping of turns.

One final comment to be made concerns the minimum practical slit width which should be used in any system. Certainly, one can obtain arbitrarily good phase resolution in one's beam by decreasing his slit width, but at the cost of decreased beam current. In fact, if one assumes that ΔR varies linearly with $\Delta\phi$, it is easy to show that the beam phase width decreases (improves) at nearly the rate at which beam current decreases as slit width is decreased, until the slit width is about the same as the zero-energy-spread beam width. This latter is just the x width of the

ellipse in Fig. 11e or f, for example, and is directly related to the source slit width. Thus, the use of phase selective slits more narrow than the source slit would probably prove to be a poor choice, giving too little beam current for the beam phase width achieved.

We now turn to one last topic, the effects of real central region electric fields, before summarizing the results of this paper.

4.2 Comparison with "Cyclone"

As mentioned in Sec. 2.2, Devil suffers from one major simplification: the neglect of the exact electric fields on the first few turns. The justification for this neglect is that such fields are different for each central region design, even for equal dee angles. It is also, of course, important to separate other influences on Q from the effects of these electric fields. However, this study could in no way be called complete without some comparison, albeit brief, of results from Devil with those from "Cyclone,"[16] an orbit code utilizing measured electric potential data for the source-puller and early turn regions.

Figure 25a gives Cyclone results for ΔR_{EO}, λ and ΔR vs. τ at $\theta=0^{o}$ for a value of $\omega_{RF}t_{o}=-22^{o}$ for the CR at the source. The E_f of 42 MeV and the central region geometry were chosen to correspond to data previously published by Blosser.[5] Devil results for this case are in Fig. 25b. ΔR_{EO} may be seen to be the same in both cases as expected since ϕ_{CR} from Cyclone agrees with ϕ_{CR} from Devil at $\theta=0^{o}$ and 180^{o} to within about 1^{o}. The Cyclone λ is smaller than its Devil counterpart by a factor of about 0.5. Note, however, that the extrema in the ΔR curves occur at similar τ values in both cases, the Cyclone values peaking near $\tau=18$ and Devil values near $\tau=14$.

The differences in λ may be traced to the more gradual nature of the energy gain on early turns in Cyclone. Our

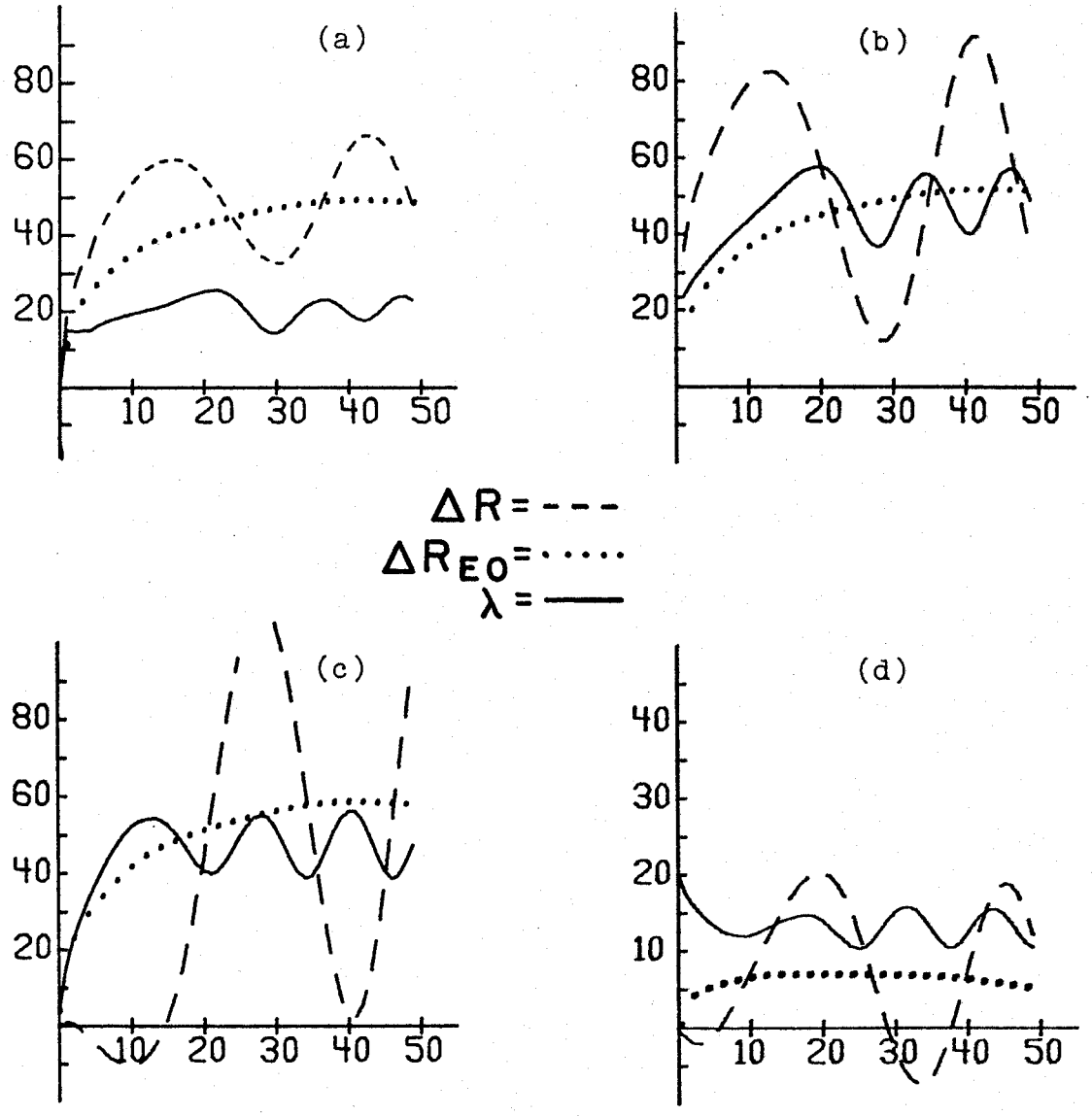

Figure 25. ΔR_{EO}, λ and ΔR vs. τ for $\theta_{or}=0^{\circ}$ plotted at $\theta=0^{\circ}$ (a,b) and $\theta=180^{\circ}$(c,d) comparing Cyclone (a) and Devil (b,c,d) results. See text, p. 100, for comparison details. Ordinate values are in mils.

picture of discrete $\delta\lambda$'s is no longer valid and must be replaced by one in which the change in λ is spread over some rotation angle at each gap crossing. But since disjunction acts only parallel to the x axis, it should be expected that the net effective $\delta\lambda$ will be less than the discrete $\delta\lambda$ we have discussed before. The discrepancy in extrema locations is also a function of the details of the electric fields. The μ_o from Cyclone has Λ about midway between the axes ($\mu_o \simeq -45^o$) while that from Devil has Λ closer to the positive x axis ($\mu_o \simeq 0^o$). This orientation difference must be made up by precession, hence the extra turns required to bring Λ parallel to the x axis, the extremal condition.

Figure 25c shows the Devil results for ΔR and its components in this 42 MeV case at $\theta=180^o$. Comparison with Fig. 3 in the work of Blosser cited above shows the same agreement as between Figs. 25a and b. Note also the exchange of node and antinode locations in ΔR between Figs. 25b and c and between Fig. 25a and Blosser's Fig. 3. This follows directly from Eq. (12) with a change in θ of 180^o. We also show Fig. 25d with ΔR and its components for a ray displaced by δp_x from the CR. This should be compared with Blosser's Fig. 5 to show that Devil and Cyclone agree on the location for a slit to eliminate spatially displaced particles.

4.3 Final Summary

We may now draw some general conclusions about the parameters affecting the longitudinal-radial coupling and the process of locating slits to perform phase selection. Q_{EO} depends mainly on $\phi_F(\tau)$ and only secondarily (10%) on form factor effects. Its maximum value and the corresponding turn number may be determined from Eq. (11) quite easily. It is quite independent of all other influences. (See Sec. 3.1.)

There are two basic influences on Q_x: the rf times at the gap crossings and the orbit asymmetry. The first determines the $\delta\lambda$'s at each gap, which latter then combine to form the $\Delta\Lambda$ over each turn (Eq. 9). The second determines the CR centering properties (x-p_x history) which in turn affect the rf times in question through Eq. (3). Orbit asymmetry also has a role in determining the K_1 and K_2 of Eq. (9). The parameters we have studied are important to phase selection to the extent that they modify one of the above influences.

Probably the parameter with the single greatest effect on phase selection is the field periodicity, N. For the two-dee cases we have restricted ourselves to, N=4 removes the orbit asymmetry term with the result that $\Delta R \simeq \Delta R_{EO}$ and $Q \simeq Q_{EO}$. N=3 involves a large orbit asymmetry term related to the gap-crossing resonance which tends to make Q_x at least comparable to Q_{EO}, thereby introducing effects which make the situation more complicated but also make

Q larger. This also means that three sector cyclotron have a definite advantage over their four sector counterparts when it comes to performing phase selection. (See Sec. 3.5.)

In particular, N=3 cases are sensitive to θ_{or}. As the dees are rotated with respect to the magnetic field, CR centering is modified, altering ϕ_{CR} and, ultimately, λ. Thus we observe as much as an order of magnitude change in λ ($\alpha=138^{o}$, h=1 and $\alpha=90^{o}$, h=3) as θ_{or} changes to sweep the dee symmetry line through one sector. $\theta_{or}=60^{o}$ tends to give the best h=1 results for most dee angles ($\theta_{or}=90^{o}$ is best for $\alpha=90^{o}$), while results on other harmonics are mixed, being highly α dependent. (See Sec. 3.1.)

Improvement in Q may be brought about in most cases by having $\phi_{F}(\tau)$ stay as large positive as possible throughout the region herein ν_{r} is close to one. This increases ΔR_{EO} and usually also λ, but exceptions there do arise ($\alpha=90^{o}$, $\theta_{or}=0^{o}$, h=1) because disjunction is not linear with ϕ_{CR}. Thus, a central field cone may be seen to be beneficial for phase selection. It should be borne in mind that having $\phi_{CR}(\tau)=0$ for all τ is not really the necessary condition for obtaining minimum final energy spread, although it is sufficient. The necessary condition is that the integral,[1]

$$\int_{0}^{E_{f}} (\sin\phi/\cos^{3}\phi)\,dE = 0.$$

Thus, large regions of large positive phase are not detrimental to final energy spread if eventually balanced by regions of negative phase. This condition is always

fulfilled by the Fielder fitting procedure. (See Sec. 3.2.)

For either N=3 or N=4, E_1 has surprisingly little effect on Q and so, given a centered beam, changing E_1 will not affect the performance of phase selection slits. (See Sec. 3.3.)

Changing acceleration harmonics mainly changes the rf gap crossing times (although this, in turn, has some effect on orbit symmetry). One should not expect, therefore, "fixed" slits to perform equally well on all harmonics at fixed α. In particular, we find that Q with $\alpha=138^{o}$ should be only slightly less on h=2 than on h=1 but with a large change in μ_o. Operation on h=3 for the dee angles examined looks to be substantially better than on h=1 because of large $\delta\phi_{CD}$ values. (See Sec. 3.4.)

Lastly, from our observations on comparing Cyclone and Devil results, we may infer that the true electric fields present in the central region act to decrease Q from the step-function-energy-gain value by decreasing λ. They also modify μ_o which controls the τ of maximum Q for fixed θ. This result serves to point out that one should include these fields in the design calculations for a slit system for an actual cyclotron. (See Sec. 4.2.)

APPENDICES

5.1 Formula Derivations

5.1.1 Calculation of the Starting Condition for an Accelerated Equilibrium Orbit

In $x\text{-}p_x$ phase space, the point representing a freely coasting particle rotates about the origin. At an accelerating gap the point jumps in the negative x direction a distance equal to the EO radial shift corresponding to the energy gain ΔE. This shift, ΔR_{EO}, is given in Sec. 2.4. Let us neglect $F(\theta)$ and assume that $(E)^{-\frac{1}{2}}$ varies negligibly over any one turn so that ΔR_{EO} depends only on ΔE. Further assuming a two dee system with dee angle α less than 180^o (one or two dees of 180^o is just a simplification of the argument below), a constant phase ϕ within a turn, harmonic h=1 and setting $E_g=qV_d$ we may write the energy gains at the gaps as

$$\Delta E_1 = \Delta E_3 = E_g \cos(\pi/2-\alpha/2+\phi) = E_g \sin(\alpha/2-\phi)$$

$$= E_g (\sin(\alpha/2)\cos\phi - \cos(\alpha/2)\sin\phi)$$

$$\Delta E_2 = \Delta E_4 = -E_g \cos(\pi/2+\alpha/2+\phi) = E_g \sin(\alpha/2+\phi)$$

$$= E_g (\sin(\alpha/2)\cos\phi + \cos(\alpha/2)\sin\phi).$$

If we define

$$\delta = A(2E_oE)^{-\frac{1}{2}} E_g \sin(\alpha/2)\cos\phi$$

$$\varepsilon = A(2E_oE)^{-\frac{1}{2}} E_g \cos(\alpha/2)\sin\phi ,$$

then the shifts ΔR_{EO} at gaps 1,2,3 and 4 are

$$\Delta R_1 = \Delta R_3 = \delta-\varepsilon$$

$$\Delta R_2 = \Delta R_4 = \delta+\varepsilon.$$

Notice that, in general, $\delta >> \varepsilon$ because $\sin \alpha/2 \geq \cos\alpha/2$ for $180^{\circ} \geq \alpha \geq 90^{\circ}$ and because $\cos\phi >> \sin\phi$ for the small phases ($<20^{\circ}$) we are interested in.

We may represent betatron oscillations with a transfer matrix formalism such that $X(\theta+\Delta\theta) = M(\Delta\theta)X(\theta)$ where $X(\theta) = x - i\eta p_x$ with $\eta = R_o/(\nu_r p)$ and approximate $M(\Delta\theta) = \exp(i\nu_r\Delta\theta)$. If ΔR_{EO} is as derived above and all drifts between gaps have the same $\nu = \nu_r$ we have, for one turn,

$$X(2\pi) = X(0)\exp(i\nu 2\pi)-(\delta-\varepsilon)\exp(i\nu(3\pi/2+\alpha/2))$$

$$-(\delta+\varepsilon)\exp(i\nu(3\pi/2-\alpha/2))-(\delta-\varepsilon)\exp(i\nu(\pi/2+\alpha/2)$$

$$-(\delta+\varepsilon)\exp(i\nu(\pi/2-\alpha/2)).$$

For an AEO, we require that $X(2\pi) = X(0)$ so we regroup the terms above and apply the relations between trigonometric and exponential functions to get

$$X(0) = -i\delta(\cos(\nu\alpha/2)/\sin(\nu\pi/2))-\varepsilon(\sin(\nu\alpha/2)/\sin(\nu\pi/2)).$$

These two terms appear as Eqs. (2) and (2a) in the text in Sec. 2.3.

One should observe that, under our assumptions, the geometry repeats after ½ turn so $X(\pi) = X(0)$ by symmetry. This condition also yields the same $X(0)$ as above.

5.1.2 Differential Energy-Gain per Turn

We assume that the particle energy gain at the i^{th} gap is

$$\delta E_i = E_g \cos(\theta_{RF} + N_i\pi)$$

where $E_g=qV_d$ is the maximum possible energy gain per gap and $N_i=0, 1, 1, 0$ for $i=1, 2, 3, 4$ with $h=1$. The difference in energy gains at the i^{th} gap between particles separated initially in phase by $\Delta\phi$ is then

$$\delta E_i = -(\Delta\phi)\ E_g \sin(\theta_{RF} + N_i\pi).$$

Over one turn, with gaps at θ_i, the total energy difference will be

$$\delta E = \sum_i \delta E_i = -(\Delta\phi) E_g \sum_i \sin(\theta_i + N_i\pi + \phi_i)$$

and over the acceleration history of the particles

$$\Delta E = -(\Delta\phi)\ E_g \sum_\tau \sum_i (\sin(\theta_i + N_i\pi) \cos\phi_i(\tau) + \cos(\theta_i + N_i\pi) \sin\phi_i(\tau)).$$

For any dee angle α, if we assume that $\phi_i(\tau)$ is small and nearly constant over any turn, we find that the first term above sums to zero. Then we may write the remainder as

$$\Delta E = -(\Delta\phi)\ E_g\ \sin(\alpha/2) \sum_{\tau} \sum_{i} \phi_i(\tau). \qquad (14)$$

If we replace $E_g \sin(\alpha/2)$ by $E_1/4$, then this result holds for any h.

We may use the Euler-Maclaurin formula to replace the sum over τ by an integral as follows:[17]

$$\sum_{\tau=\tau_j}^{\tau_f} \phi_i(\tau) \simeq \int_{\tau_j}^{\tau_f} \phi_i(\tau)\ d\tau + \tfrac{1}{2}(\phi_i(\tau_j)+\phi_i(\tau_f)).$$

In the cases we are interested in, $\tau_j=0$ and τ_f is usually greater than 15 so that $\int \phi_i(\tau)\ d\tau >> \phi_i(\tau_j)$ and $\phi_i(\tau_f)\simeq 0$.

If we recognize that $\phi_F(\tau)$ is nearly the average value of the $\phi_i(\tau)$ over one turn and replace $E_g \sin(\alpha/2)$ by $E_1/4$, Eq. (7) in Sec. 2.5 follows immediately from Eq. (14).

5.2 The code "Devil"

"Devil" is a code for calculating median plane orbits and deviations between them using a fourth order Runga-Kutta-Gill integration technique with roundoff error correction.[18] It is similar to the code "Goblin-4" written for this laboratory by D. Johnson, while incorporating improvements in technique over Goblin and performing direct comparisons of the orbits of up to nine rays. Devil can also plot its results. It does give up Goblin's ability to "accelerate" a ray backward and does not include provision for calculating axial motion. Like Goblin, Devil assumes a step-function energy gain at each gap. Following are the equations of motion solved by Devil, the program flow and the input parameters with definitions, units and FORTRAN formats.

The input to the code consists of the "standard" magnetic field deck (suitable for use in all M.S.U. orbit codes now in general use) followed by a string of running parameters defining the condition of the machine and the particle source location. The field deck defines the following quantities:

E_o = particle rest energy ($=m_o c^2$) (MeV)

q = particle charge (units of e)

N = number of field sectors

n = number of field harmonics in deck

$$B_o = B(r=0) \quad (kG)$$

$$A = c/\omega_o$$

$$\omega_o = qB_o/(m_o c) \quad (MHz)$$

Note that A, B_o and ω_o are not independent. If A is specified the code assumes that B_o and ω_o are also. Otherwise Devil calculates its own self-consistent set of constants. The field is specified by the coefficients in its Fourier decomposition:

$$B(r,\theta) = B(r) + \sum_{j=1}^{m} (H_j(r)\cos(jN\theta) + G_j(r)\sin(jN\theta)).$$

The running parameters are listed in full with proper units and formats on the last three pages of this section. The rf frequency is set by defining an ε_{rf} such that

$$\omega_{RF} = \omega_o (1+\varepsilon_{rf})h.$$

Devil performs its calculations in terms of modified cyclotron units so that r, p_r and $B(r,\theta)$ are in units of inches, $m_o c/A$ and B_o, respectively. In these units the equations of motion are:[13]

$$\gamma \equiv 1+E/E_o$$

$$P \equiv (p^2-p_r^2)^{\frac{1}{2}}$$

$$dr/d\theta = rp_r/P$$

$$dP_r/d\theta = P - rB(r,\theta)$$

$$d\theta_{rf}/d\theta = h(1+\varepsilon)\gamma r/P$$

The energy gain at the i^{th} gap is

$$\Delta E_i = q\ V_d \cos\ (\theta_{rf}(\theta_i) + N_i\pi),$$

where $N_i = 0,1,h,h+1$ for i=1,2,3,4. The gap locations, θ_i, are given by

$$\theta_1 = \theta_{or} + \alpha_1,$$

$$\theta_2 = \theta_{or} + \pi - \alpha_2,$$

$$\theta_3 = \theta_{or} + \pi + \alpha_2,$$

$$\theta_4 = \theta_{or} - \alpha_1,$$

where the α of Sec. 2.2 is $\alpha = \pi-\alpha_1-\alpha_2$. We have used only $\alpha_1=\alpha_2$ in this paper.

The program begins with the computation of EO properties R_{EO} and P_{REO} vs. energy at each output azimuth using the code "Sigma-EO"[11] as a subroutine. The angular steps to be used in the integration are determined and the total field at the end and mid-points of each step are calculated and stored. The rays (the CR is always included) are "accelerated" a specified number of turns one at a time, results at the angles of interest being stored until all rays are finished. Then x and p_x values are obtained using the tabulated EO data, deviations from the CR in ϕ, r, R_{EO}, x and p_x are found and stored and a printed record of ϕ, E, r, p_r, x, p_x and the above deviations is output. Finally, these deviations are plotted if desired. This modular program form is adopted to trade core storage for computing speed, a worthwhile endeavor on the M.S.U.

Cyclotron Lab's XEROX SIGMA-7 computer, which has 64K words of real core. Average running time accelerating five rays for 50 turns with six output azimuths and creating three plots is about 7.5 minutes.

Devil Input

Standard field deck

Card Format

A. (F7.2, F11.3, I3, 3F11.6)

1. Field identification number
2. Particle rest energy (MeV)
3. Particle charge (e)
4. Cyclotron field unit (kG)
5. Cyclotron length unit (in.)
6. Ideal isochronous frequency (MHz)

B. (2I3, 2F11.6, I4)

1. Number of sectors
2. Number of field harmonics to follow
3. First radius value in field tables (in.)
4. Radius increment between table entries (in.)
5. Number of table entries

C. (7F11.7)

Tables of $B(r)$, $H_j(r)$, $G_j(r)$

D. (2I3)

1. Number of imperfection harmonics to follow.
   =0, none read, skip to next input
2. Imperfection harmonic number

E. (7F11.7)

Imperfection harmonics (if any)

Running parameters - each parameter on a separate card

F. (2I2, F12.5)

0 1 Frequency scale factor, default=1

0 2 ε_{rf}

0 3 Acceleration harmonic

0 4 Dee-To-Ground Voltage (kV)

0 5 θ_{or}

0 6 α_1

0 7 α_2

0 8 Phase constant for h≠1, default=90°(h=2), -180°(h=3)

0 9

010 Ray ID (see below) at Λ vector origin

011 Ray at Λ vector head

012 Number (maximum=6) of plotting angles to follow
-0, no plotting done, skip to next input
a.) (4A4) Plot Title
b.) (7F11.5) Plotting angles (degrees)

013 Number (maximum=105) of values in following EO table
=0, no table follows, skip to next input
a.) (F11.5) Angle for which EO data is presented
b.) (3F12.5) EO table (E, R_{EO}, P_{REO})

014 Number (maximum=16) of extra printing angles to follow.
Dee gaps are automatically included.
a.) (7F11.5) Output angles

Initial (source) conditions

G. (2I2, F12.5)

ID, IN, Z
where
ID = Ray identification number
= 1 implies CR (value of Z copied into variable IN for all other rays when this ID occurs)
IN = Variable index

= 1 Azimuth (deg.)
= 2 Radius (in.)
= 3 Radial momentum (in.)
= 4 Starting phase (deg.)
= 5 Energy (MeV)

Z = Variable value

(Note: Z replaces the CR value if ID≠1 and IN=0. However, Z adds to the CR value if ID≠1 and IN<0.)

H. (I2)

Run command = -1 begins calculations

LIST OF REFERENCES

REFERENCES

1. M. M. Gordon, "Single Turn Extraction," IEEE Trans. Nucl. Sci. NS-13 (4), 52(1966).

2. H. G. Blosser, M. M. Gordon and T. I. Arnette, "Resonant Extraction from Three-Sector Low-Spiral Cyclotrons," Nucl. Instr. and Meth. 18-19, 488(1962).

3. H. G. Blosser, "Problems and Performance in the Cyclotron Central Region," IEEE Trans. Nucl. Sci. NS-13 (4),1(1966)

4. H. G. Blosser, "Performance of a Modern Medium Energy Cyclotron," Bull. Am. Phys. Soc., (Nov. 1967).

5. H. G. Blosser, "Optimization of the Cyclotron Central Region for the Nuclear Physics User," Fifth International Cyclotron Conference (Butterworths, London, 1971), 257.

6. D. W. Kerst and R. Serber, "Electronic Orbits in the Induction Accelerator," Phys. Rev. 60, 53(1941).

7. E. D. Courant and H. S. Snyder, "Theory of the Alternating-Gradient Synchrotron," Ann. Phys. (N.Y.) 3, 1(1958).

8. M. M. Gordon, "Orbit Properties of the Isochronous Cyclotron Ring with Radial Sectors," Ann. Phys. (N.Y.), 50, 571(1968).

9. A. J. Lichtenberg, Phase Space Dynamics of Particles. (John Wiley & Sons, Inc., New York, 1969), p. 119.

10. M. M. Gordon and D. A. Johnson, "Application of a New Field Trimming Program to the M.S.U. Cyclotron," AIP Conf. Proc. 9, 298(1972).

11. M. M. Gordon, T. I. Arnette and D. A. Johnson, Bull. Am. Phys. Soc., (April, 1964).

12. M. M. Gordon, "The Electric Gap-Crossing Resonance in a Three Sector Cyclotron," Nucl. Inst. and Meth. 18-19, 268(1962).

13. H. S. Hagedoorn and N. F. Verster, "Orbits in an AVF Cyclotron," Nucl. Instr. and Meth. 18-19, 201(1962).

14. J. S. Balduc and G. H. Mackenzie, "Some Orbit Calculations for TRIUMF," IEEE Trans. Nuc. Sci. NS-18 (3), 287(1971).

15. L. L. Learn, H. G. Blosser and M. M. Gordon, "An Optimized Multi-Particle Central Region for the Michigan State University Isochronous Cyclotron," AIP Conf. Proc. 9, 291(1972).

16. L. L. Learn, D. A. Johnson, private communication.

17. P. J. Davis and P. Rabinowitz, Numercial Integration, (Blaisdell Pub. Co., Waltham, Mass., 1967), p. 84.

18. R. W. Hamming, Numerical Methods for Scientists and Engineers, (McGraw-Hill Book Co., N.Y., 1962), p. 212.